LA-UR 88-3118

DTIC FILE COPY

(2)

Los Alamos National Laboratory is operated by the University of California for the United States Department of Energy under contract W-7405-ENG-36

AD-A201 298

TITLE EARLY TIME STRUCTURING AT VERY HIGH ALTITUDES: INSTABILITY MECHANISM, PROPERTIES AND CONSEQUENCES

AUTHOR(S) Dan Winske, X-1

SUBMITTED TO Report prepared for the Defense Nuclear Agency under Project Code RB, Task Code RC, Work Unit 167

DTIC ELECTE OCT 1 9 1988 S D H

By acceptance of this article, the publisher recognizes that the U.S. Government retains a nonexclusive, royalty-free license to publish or reproduce the published form of this contribution, or to allow others to do so, for U.S. Government purposes

The Los Alamos National Laboratory requests that the publisher identify this article as work performed under the auspices of the U.S. Department of Energy

Los Alamos National Laboratory
Los Alamos, New Mexico 87545

FORM NO. 836 R4
ST. NO. 2629 5/81

DISTRIBUTION STATEMENT A
Approved for public release;
Distribution Unlimited

88 10 18 161

REPORT DOCUMENTATION PAGE

1a. REPORT SECURITY CLASSIFICATION UNCLASSIFIED	1b. RESTRICTIVE MARKINGS
2a. SECURITY CLASSIFICATION AUTHORITY	3. DISTRIBUTION / AVAILABILITY OF REPORT Approved for public release, distribution is unlimited
2b. DECLASSIFICATION / DOWNGRADING SCHEDULE	
4. PERFORMING ORGANIZATION REPORT NUMBER(S) LA-UR-88-3118	5. MONITORING ORGANIZATION REPORT NUMBER(S)
6a. NAME OF PERFORMING ORGANIZATION Los Alamos National Laboratory	6b. OFFICE SYMBOL (If applicable) X-1
7a. NAME OF MONITORING ORGANIZATION	
6c. ADDRESS (City, State, and ZIP Code) Los Alamos, New Mexico 87545	7b. ADDRESS (City, State, and ZIP Code)
8a. NAME OF FUNDING / SPONSORING ORGANIZATION Defense Nuclear Agency	8b. OFFICE SYMBOL (If applicable) RAAE
9. PROCUREMENT INSTRUMENT IDENTIFICATION NUMBER	
8c. ADDRESS (City, State, and ZIP Code) Washington DC 20305-1000	10. SOURCE OF FUNDING NUMBERS PROGRAM ELEMENT NO.: RAAE; PROJECT NO.: RB; TASK NO.: RC; WORK UNIT ACCESSION NO.: 167

11. TITLE (Include Security Classification)
EARLY TIME STRUCTURING AT VERY HIGH ALTITUDES: INSTABILITY MECHANISM, PROPERTIES, AND CONSEQUENCES

12. PERSONAL AUTHOR(S)
D. Winske

13a. TYPE OF REPORT	13b. TIME COVERED	14. DATE OF REPORT (Year, Month, Day)	15. PAGE COUNT
Technical	FROM 10/87 TO 10/88	88 September 15	52

16. SUPPLEMENTARY NOTATION
This work was supported by the Defense Nuclear Agency under Project Code RB, Task Code RC, Unit Work Code 167, Unit Work Title: Simulations and Modeling of HANE/VHANE

17 COSATI CODES		
FIELD	GROUP	SUB-GROUP

18. SUBJECT TERMS (Continue on reverse if necessary and identify by block number)
Laser Experiment
Early time structuring
Particle simulations
Flute instability

19. ABSTRACT (Continue on reverse if necessary and identify by block number)

This report considers structuring that results from plasma streaming at sub Alfvenic speeds across an external magnetic field, as might occur in a very high altitude nuclear explosion (VHANE). In previous reports we have proposed the lower hybrid drift instability enhanced by the deceleration of the plasma by the field produces the flute modes observed on the surface of expanding laser produced plasmas. We have derived an appropriate dispersion equation to describe the properties of the unstable waves and carried out particle simulations to show the growth and evolution of the instability. We review the salient features of this earlier work and then describe recent additions and refinements to the theory and simulations. We discuss improvements to the dynamics of a 3-D expansion, some initial work on a nonlocal linear theory, the addition of finite electron beta effects to the linear theory, the scaling of the wave properties with the ratio of the ion gyroradius to the magnetic confinement radius, and a better understanding of the nonlinear evolution of the instability. Furthermore, we have considered nonsymmetric expansions, simulations of the instability in 3-D, the very weak limit of the instability, and the effect of collisions. Next, the consequences of these results both for the NRL laser experiment as well as other experiments and for VHANEs are considered. A comparison of the linear and nonlinear properties of the waves observed in the simulations with those seen in the laser experiments is carried out and issues which further experiments might resolve are outlined. Finally, the scaling of the results presented here to the much weaker instability regime expected in a VHANE is discussed.

20. DISTRIBUTION / AVAILABILITY OF ABSTRACT	21. ABSTRACT SECURITY CLASSIFICATION
☒ UNCLASSIFIED/UNLIMITED ☐ SAME AS RPT. ☐ DTIC USERS	UNCLASSIFIED

22a. NAME OF RESPONSIBLE INDIVIDUAL	22b. TELEPHONE (Include Area Code)	22c. OFFICE SYMBOL
Dan Winske	505-667-2868	X-1

DD FORM 1473, 84 MAR 83 APR edition may be used until exhausted. All other editions are obsolete.

SECURITY CLASSIFICATION OF THIS PAGE

UNCLASSIFIED

Early Time Structuring at Very High Altitudes: Instability Mechanism, Properties, and Consequences

Dan Winske

Applied Theoretical Physics Division

Los Alamos National Laboratory

September 1, 1988

Abstract

This report considers structuring that results from plasma streaming at sub Alfvenic speeds across an external magnetic field, as might occur in a very high altitude nuclear explosion (VHANE). In previous reports we have proposed the lower hybrid drift instability enhanced by the deceleration of the plasma by the field produces the flute modes observed on the surface of expanding laser produced plasmas. We have derived an appropriate dispersion equation to describe the properties of the unstable waves and carried out particle simulations to show the growth and evolution of the instability. We review the salient features of this earlier work and then describe recent additions and refinements to the theory and simulations. We discuss improvements to the dynamics of a 3-D expansion, some initial work on a nonlocal linear theory, the addition of finite electron beta effects to the linear theory, the scaling of the wave properties with the ratio of the ion gyroradius to the magnetic confinement radius, and a better understanding of the nonlinear evolution of the instability. Furthermore, we have considered nonsymmetric expansions, simulations of the instability in 3-D, the very weak limit of the instability, and the effect of collisions. Next, the consequences of these results both for the NRL laser experiment as well as other experiments and for VHANEs are considered. A comparison of the linear and nonlinear properties of the waves observed in the simulations with those seen in the laser experiments is carried out and issues which further experiments might resolve are outlined. Finally, the scaling of the results presented here to the much weaker instability regime expected in a VHANE is discussed.

1. Introduction

Structure formation at early times remains an important issue for high altitude nuclear explosions. At low altitudes the coupling of the debris plasma to the background occurs through collisional processes, and the front edge of the resulting blast wave may be subject to Rayleigh-Taylor type instabilities [Brecht and Papadopoulos, 1979]. At higher (e.g., STARFISH) altitudes, collisionless plasma processes take over with the generation of a high Mach number shock wave and structure on the ion gyroradius scale [Thomas and Brecht, 1986]. At even higher altitudes, the so called VHANE regime, the Alfven Mach number of the debris falls below unity and only a weak shock, if any, is produced. Because of the lack of actual test data in this regime, laboratory and space experiments as well as computer simulations provide a method to address the question of early time structure formation at very high altitudes.

At STARFISH-like altitudes the debris gives up its energy and momentum when it has overrun an equivalent mass of air ions. At higher altitudes, where the air density is much less, the debris loses energy expanding against the geomagnetic field. The revelant distance over which the debris comes to rest is the magnetic confinement radius, R_B. As the bomb plasma expands, it drags the magnetic field along, creating a diamagnetic cavity of radius $\sim R_B$.

Diamagnetic cavities also occur in space, both artifically and naturally. The artificial cavities result from chemical releases, such as the AMPTE (Active Magnetospheric Particle Tracer Explorers) mission in which small cannisters of lithium and barium were exploded in the solar wind, the magnetosheath, and the magnetotail [Krimigis et al., 1982]. Natural cavities are observed infrequently upstream of the Earth's bow shock [Thomsen et al., 1986]. They occur as a result of changing conditions in the solar wind that momentarily allow a large fraction of the incoming ions to be reflected by the bow shock and propagate back upstream [Thomsen et al., 1988]. Magnetic field-free cavities are also formed around the nucleus of a comet [Mendis and Houpis, 1982], where a large number of emitted neutrals become ionized and exclude the field. Diamagnetic cavities are also produced in the laboratory by means of laser produced plasmas expanding against an externally applied magnetic field. [Okada et al., 1981; Ripin et al., 1987; Zakharov et al., 1986].

Generally, "small" plasmas, where small means the ion gyroradius ρ_i based on the expansion velocity and the external magnetic field is comparable to or greater than R_B, tend to show observable, field aligned instabilities (structures) [e.g., laser experiments (Ripin et al., 1987; Okada et al., 1981), theta-pinch implosions (Keilhacker et al., 1974), plasmoid propagation studies (Papadopoulos et al., 1988; Wessel et al., 1988), AMPTE releases (Bernhardt et al., 1987)], while "large" plasmas with $\rho_i \ll R_B$ [diamagnetic cavities at the bow shock [Thomsen et al., 1986] and the cometary cavity at Comet Halley [Neubauer, 1987] do not. We later show that this follows from the properties of the instability involved and thus conclude that structure of this type is not likely to be important for the very large VHANE plasma.

The experiments which do show structure yield important information about the instability which generates it. In the AMPTE experiments several kg of barium were released in the Earth's magnetotail and the expanding cloud was observed optically from the ground [Bernhardt et al., 1987]. The plasma expanded to a final radius $R_B \sim \rho_i \sim 200$ km, while short wavelength ($\lambda \sim 40$ km) field aligned (flute) modes appeared as ripples on the surface near the time of maximum expansion. The structures did not appear to move, suggesting real frequency $\omega_r \sim 0$, or to change mode number as the cloud began to collapse. The surface waves observed in the NRL laser experiments [Ripin et al., 1987] were often more prominent, in that the radial extent of the fingers was larger and a smaller number of modes was present. The wavelengths were still short, $\lambda < \rho_i$, and again the modes appeared to be time stationary. High frequency (~ 500 MHz) noise corresponding to roughly the lower hybrid frequency was also detected, as has been found at the edge of the barium cloud by the AMPTE/IRM satellite [Gurnett et al., 1986]. Furthermore, as the external magnetic field was changed in the laser experiments, the wavelengths of the modes did not seem to be affected. The surface structures could also been followed later in time, into their apparent nonlinear stage. The tips of the flutes were observed to freestream ahead of the plasma, tended to bend in the electron cyclotron sense in the magnetic field, and sometimes seemed to bifurcate into shorter wavelength modes. The surface waves seen in the Japanese laser experiments [Okada et al., 1981] were more like the AMPTE release in that they appeared at the time of maximum expansion and then dissappeared rather quickly. Although they were also time stationary, unlike the NRL results, the observed wavenumbers (k) had a strong dependence on the applied magnetic field, $k \sim B^{0.8}$. Again, lower hybrid noise was detected. Finally, experiments of a similar nature have been carried out by Zakharov et al. [1986]. It is not clear whether they observed the surface waves visually, but for small plasmas ($\rho_i > R_B$) the size of the magnetic cavity was significantly less than R_B, and intense high frequency electric noise was detected, again suggesting a strong instability in this regime.

The observations have stimulated various theoretical investigations to understand the instability that gives rise to the structure. Sydora et al. [1983] consider a diocotron-like instability driven by relative drifts of electrons in nearby charge layers, although Akimoto et al. [1988] show that the inclusion of the ion dynamics in such a model greatly reduces the growth of the mode. The fact that the instability appears even in the absence of a thin plasma ring is also contrary to the assumptions of the diocotron model. Peter et al. [1983] derive expressions for the properties of a kinetic Rayleigh-Taylor instability, using a sharp boundary analysis. Hassam and Huba [1987, 1988] emphasize the importance of the slowing of the plasma by the magnetic field and include the ion inertia term in a set of modified MHD equations. Characteristics of the instability in the long wavelength limit appropriate to their model have been derived; the non-Rayleigh-Taylor-like nature of the mode has also been stressed. Okada et al. [1979] and later Winske [1988] and Galvez et al. [1988] have included both ion and electron dynamics and argued that the instability in question is the lower hybrid drift instability enhanced by the deceleration of the expanding plasma. The inclusion of electron effects give a physical, short wavelength cutoff and a peak in the growth rate as a well defined wavenumber. Both Okada et al. [1979] and Galvez et al. [1988] consider the electrostatic limit with finite temperatures for both the electrons

DTIC COPY INSPECTED 1

n For
&I
ed
tion
tion/
ility Codes
il and/or
Dist Special
A-1

and ions. Winske [1988] includes electromagnetic corrections but takes the electrons as cold. Generally, the wavenumbers at maximum growth calculated from these models that include electron effects are a factor of 3-30 too large to explain the observations. Okada et al. [1981] compare with their laser experiments, while Winske [1988] and Galvez et al. [1988] with the AMPTE magnetotail releases. There are, however, a number of other effects that can be included in the analysis which improve the agreement. A discussion of these issues comprises a major portion of this report.

Furthermore, the experiments and theory have been supported by a number of simulations of plasmas expanding against an ambient magnetic field. Two-dimensional electrostatic particle simulations which show structure, but no development of a diamagnetic cavity, have been carried out by Sydora et al. [1983] and Galvez et al. [1988]. Electromagnetic particle simulations displaying cavity formation have been done by Gisler [1988] and Winske [1988]. Gisler's simulations were done in the plane containing B and show no instability; Winske's runs were in the plane perpendicular to B and show the structure formation, although they do not include the dynamics along the field direction that Gisler studies. Other simulations have been done with the electrons treated as a fluid: Sgro et al. [1988] including electron inertia, Brecht and Thomas [1988] with massless electrons, and Huba et al. [1987] with a single fluid (including the Hall term). All three simulations show the development of the instability, even though the geometry was different (Sgro et al. [1988] and Huba et al. [1987] in a slab geometry instead of the more conventional cylindrical expansion) as are the characteristic wavelengths of the modes (determined to some degree by the cell size used in the computations). The net conclusion is that the instability is a very robust beast. The fact that it occurs in a variety of simulations which have different physical models suggests that it can be investigated from many theoretical points of view. We stress that while the various approaches tend to emphasize different aspects and often give a different name to the instability, the underlying physical mechanism is basically the same.

The purpose of this report is to summarize DNA sponsored research at Los Alamos related to the early time structuring problem at very high altitudes. We begin with a review of the basic physics model, results from linear analysis, and the simulations. Details of this work can be found in Winske [1987, 1988] and Akimoto et al. [1988]. We then discuss a number of enhancements to the theory and recent simulation work which bears on the problem. Specifically, we describe additions to the basic model which include an improved treatment of the dynamics of the expansion, the addition of electron kinetic effects to the linear theory, and some work on a nonlocal linear analysis. Related to the simulations, we have done a careful study of ρ_i/R_B scaling, an analysis of nonlinear mode coalescence, some work on asymmetric expansions, and a preliminary study of additional physics that occurs in three-dimensional simulations. We have also considered the weak limit of the instability and included the effect of collisions in both the linear theory and the simulations. Finally, the application of this work to the laser experiments at NRL and VHANEs is addressed. The key question related to the laser experiment involves the scaling of the instability as a function of parameters such as the applied magnetic field, ρ_i/R_B, and the asymmetry of the expansion. We also discuss long time effects, such as bifurcation of the tips of the

structures, and how the properties of the structure change with the background pressure (i.e., collisions). For VHANEs the principal issue involves the strength of the instability and its effect on the size of the diamagnetic cavity, the confinement of the debris plasma, and the amount of electron and ion heating. The results of such studies can then be used as input for longer time scale calculations that follow the evolution of the disturbed atmosphere for many hours after the explosion.

2. Review of Basic Instability Mechanism, Linear Theory and Simulations

We begin with a review of the basic physics of the instability and some results of linear analysis and simulations. Much of this work is explained in more detail in earlier reports [Winske, 1987, 1988]. Later sections discuss recent refinements to this earlier work as well as its relation to the structuring seen in the laser experiments and possible consequences for VHANEs.

The physics of the instability is shown in Figure 1. We consider a debris plasma expanding, either thermally or with a directed velocity, against an ambient magnetic field, B_o. For the discussion here, we consider only the expansion across the magnetic field; 3-D effects will be discussed in Section 3A and 3G. On a time scale short compared to the ion cyclotron period, $\Omega_i t < 1$ (ion cyclotron frequency $\Omega_i = eB_o/m_i c$, where e is the electronic charge, m_i is the ion mass, and c is the speed of light), the ions can be considered unmagnetized and thus expand radially outward. The electrons, tied to the magnetic field, try to hold the ions back, giving rise to a radially inward pointing electric field, E_r. As the ions on the outer edge are slowed by E_r, the ions inside catch up, compressing the plasma into a thin shell. The electrons and magnetic field are also compressed, forming a diamagnetic cavity. Because the electrons are magnetized, they $\vec{E} \times \vec{B}$ drift azimuthally relative to the ions. This current (I) is, of course, in the right sense to generate a magnetic field opposite to the applied field inside. It is the relative electron-ion drift in the shell which is the free energy source for the instability.

The simplest way to carry out a linear analysis of the perturbations is a local theory, where the radial dependence of the modes is neglected. A nonlocal approach is described in Section 3B, where we discuss the physical regime in which each is valid. One considers unmagnetized ions and magnetized electrons drifting azimuthally with respect to the ions with velocity V_E in a uniform magnetic field. To get V_E we use the fact that the radial electric field

$$eE_r = -m_i g - T_i \epsilon_n \tag{1}$$

where $g = -dV_{ir}/dt (> 0)$ is the deceleration of the ions, T_i is the ion temperature, and $\epsilon_n = -n_i^{-1} dn_i/dx (> 0)$ is the density gradient. V_E is thus

$$V_E = -\frac{cE_r}{B_o} = \frac{m_i c g}{eB_o} + \frac{T_i c}{eB_o}\epsilon_n = V_g + V_n \tag{2}$$

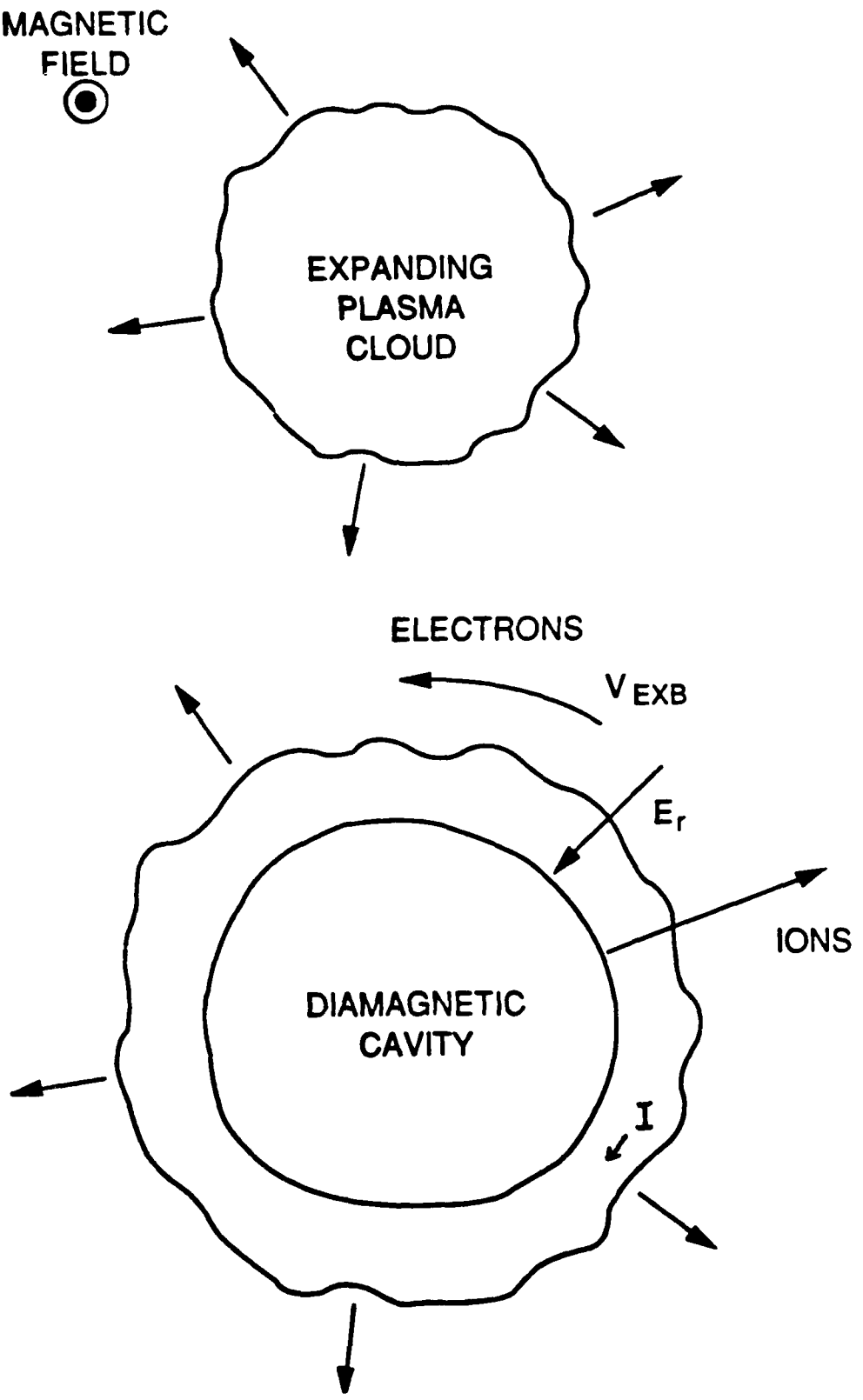

Figure 1. Schematic of the structuring mechanism showing the outward motion of the ions, the radial electric field, the electron $\vec{E} \times \vec{B}$ drift, the resulting current (I), and the diamagnetic cavity.

The second term due to the ion pressure gradient is the usual driving term for the lower hybrid drift instability [e.g., Davidson and Gladd, 1975]. For most applications, where it has been studied, e.g., theta pinches, the contribution of the deceleration is small ($V_g \ll V_n$) and ignored. As we shall see, the situations of interest here, when the instability generates large scale structures, is characterized by $V_g \geq V_n$. As with earlier work [Davidson and Gladd, 1975; Okada et al., 1979; Winske, 1988], we will continue to use the name lower hybrid drift instability when $V_g \neq 0$, in particular even when $V_g \geq V_n$.

The resulting dispersion equation can be written down in various forms, depending on what other effects are included. For example, limiting the perturbations to being electrostatic and including $T_e \neq 0$ gives the electrostatic limit [Eq. (2) of Okada et al. (1979) or Eqs. (A.1-A.8) of Galvez et al. (1988)]. Winske [1988] (Eq. 20) includes electromagnetic effects but $T_e = T_i = 0$. This latter form is convenient for making analytic approximations and in showing that the instability persists in the long wavelength ($k \rightarrow 0$) limit where charge neutrality and massless electrons are assumed. The scaling that results in this case is equivalent to that of Hassam and Huba [1987] and explains why the instability occurs in hybrid simulations with $m_e = 0$ [Brecht and Thomas, 1988] as well as in single fluid Hall MHD codes [Huba et al., 1987] with maximum growth usually occurring at the shortest allowable wavelengths in the calculations.

Figure 2 displays solutions of the linear dispersion equation [Eq. (28) of Winske (1988)] for $V_g = 0$, corresponding to the usual lower hybrid drift instability, for $T_e = 0$. (Other parameters are: $\epsilon_n c/\omega_i = 10$, $\omega_i^2 = 4\pi n_i e^2/m_i$, $\beta_i = 8\pi n_i T_i/B_o^2 = 0.2$ so that $V_n/v_A = 1$, $v_A^2 = B_o^2/4\pi n_i m_i$ with $m_i/m_e = 1836$ and $v_A/c = 1/200$). The real (ω_r, solid curve) and imaginary (γ, dashed curve) parts of the frequency are plotted versus wavenumber. For convenience, the frequencies are normalized in terms of Ω_i and k in terms of kc/ω_i. Growth of the instability persists down to $k \rightarrow 0$, where $\gamma \gg \omega_r$, but peaks at shorter wavelengths, $kc/\omega_i \sim 150$, implying $kc/\omega_e \sim 4$, with $\gamma \sim \omega_r \sim 30\Omega_i \sim 0.8\omega_{LH}$, where the lower hybrid frequency is defined as $\omega_{LH}^2 = \omega_i^2/(1+\omega_e^2/\Omega_e^2) \sim \Omega_e\Omega_i$. In contrast, Figure 3 shows results (with same scales) for the same parameters except that $V_g/v_A = 3$. Maximum growth of the instability is now larger (about a factor of two) and occurs at smaller wavenumbers (about a factor of two), with again $\omega_r \sim \gamma$ at maximum growth and $\omega_r \ll \gamma$ at smaller k.

Analytic expressions for γ and k corresponding to maximum growth can also be derived [Winske, 1987, 1988]. For example, assuming $V_g \gg V_n$ one finds

$$k = \omega_{LH}(\epsilon_n/g)^{1/2} \tag{3}$$

and

$$\frac{\omega}{\omega_{LH}} = \frac{(\epsilon_n c/\omega_i)^{1/2}}{(V_g/v_A)^{1/6}} \frac{1+i\sqrt{3}}{2} \tag{4}$$

Relating g to initial conditions assuming a 2-D expansion [Winske, 1988] yields

$$g = V_D \frac{c}{r_o} \frac{\Omega_i}{\omega_c} \tag{5}$$

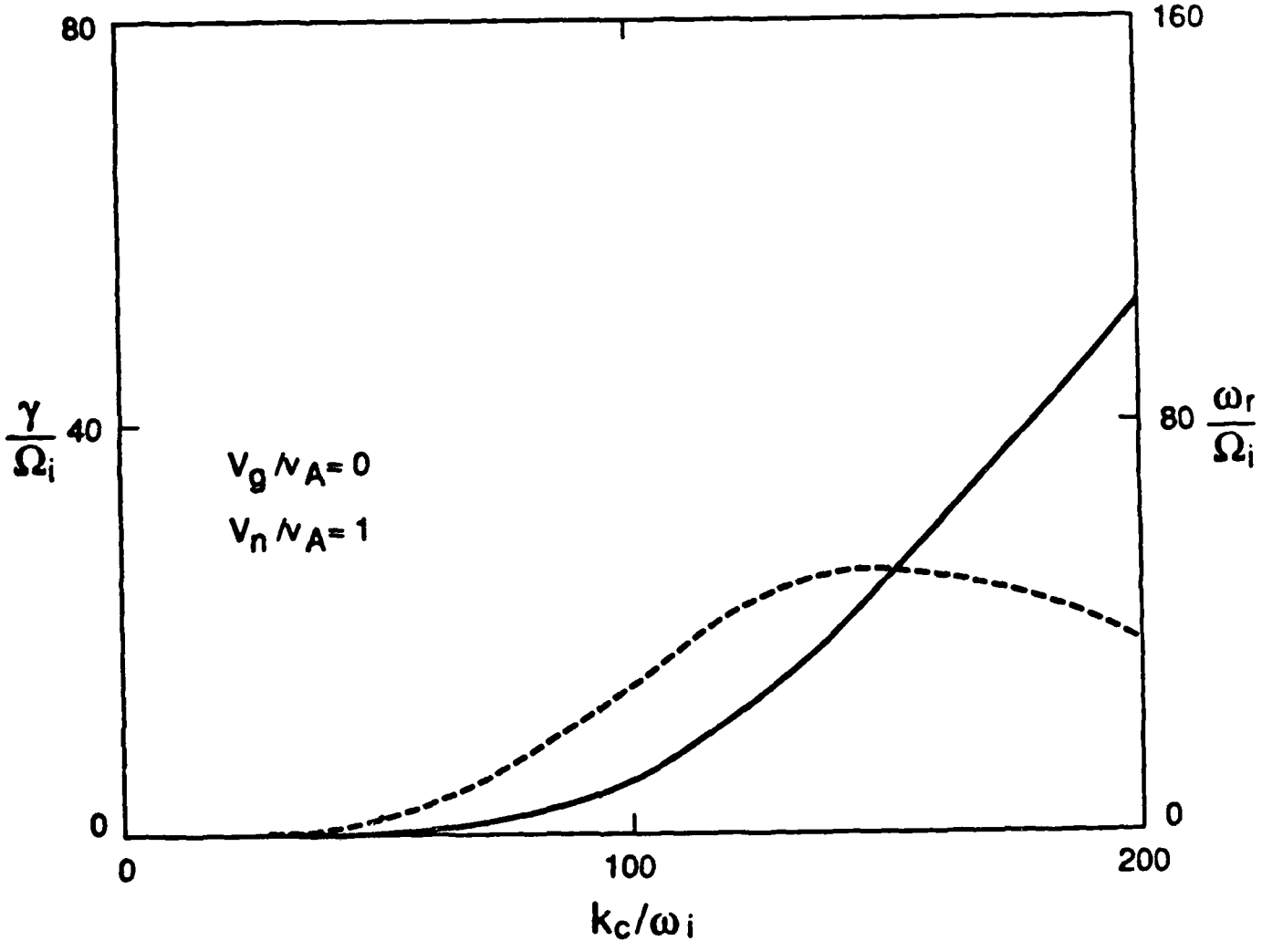

Figure 2. Results of linear theory for the usual lower hybrid drift instability ($V_g = 0$, $V_n/v_A = 1$, $\beta_i = 0.2$) showing real (ω_r, solid curve) and imaginary (γ, dashed curve) parts of the frequency versus wavenumber k.

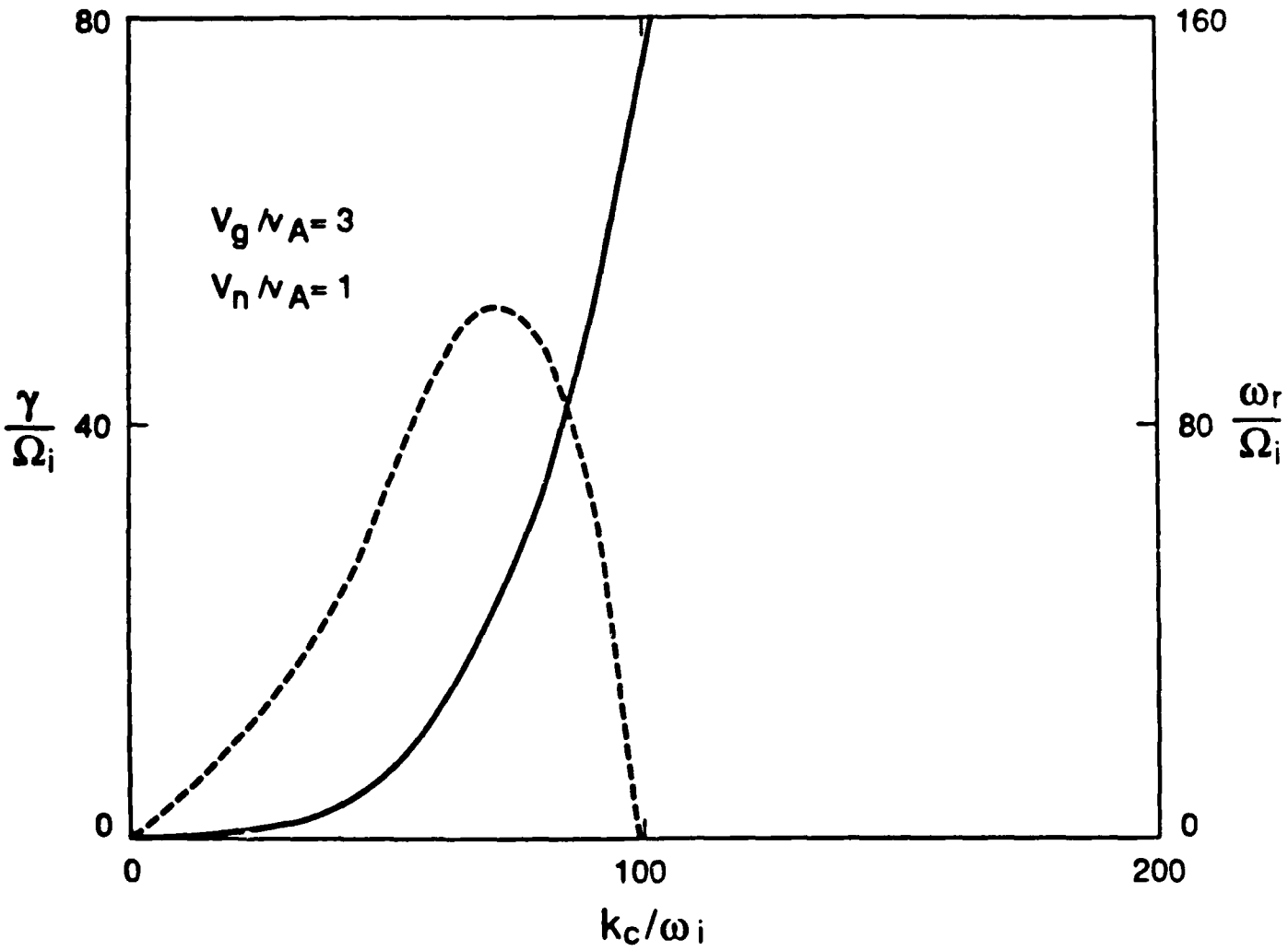

Figure 3. Same as Figure 2, but $V_g/v_A = 3$, showing enhancement of the instability when the plasma is decelerated by the magnetic field.

where V_D is the initial expansion velocity, r_o is the initial plasma radius, and ω_c is the ion plasma frequency using the initial density. Then Eq. (3) becomes

$$\frac{kc}{\omega_e} \sim (\frac{\epsilon_n r_o c}{V_D})^{1/2} (\frac{\Omega_e}{\omega_e})^{1/2} (\frac{m_e}{m_i})^{1/4} \tag{6}$$

an expression that will be checked by simulations, shortly.

Next, some results of simulations that confirm this basic picture will be shown. Figure 4 displays snapshots of ion density contours from a two-dimensional electromagnetic particle simulation at various times, similar to those described in Winske [1987, 1988]. The plasma initially forms a dense column ($r_o = 2c/\omega_e$) which expands with a velocity $V_D = 0.005c$ into a vacuum. The ambient magnetic field (magnitude given by $\Omega_e/\omega_e = 0.4$) is perpendicular to the plane of the simulation. The ions have mass $m_i/m_e = 1600$ and thermal speed $v_i = (2T_i/m_i)^{1/2} = 0.005c$; the electron thermal speed is $v_e = 0.05c$. As the plasma expands, the deceleration tends to compress the cloud into a shell on which flutes appear. By $\omega_{LH}t = 4$, the expansion stops. At later times, most of the ions start to recompress, although the plasma on the outer edge continues to move radially outward. By counting ripples on the surface, one finds that the short wavelength modes appeared to have coalesced into longer wavelength structures at later times. Although there is not much azimuthal motion of the perturbations, we later show that the frequency of the short wavelength modes is $\sim \omega_{LH}$.

While the results look qualitatively similar to runs presented in the earlier reports, there are some quantitative differences. Before, the modes tended to be short in wavelength, at about the shortest resolvable by the grid. At later times there was more diffusion across the field and little evidence for coalescence. The present runs generally use hotter plasmas, which tend to increase the wavelength and slow the growth of the instability. As a consequence, the waves of interest are well resolved and the plasma reaches maximum expansion radius without strong diffusion across the magnetic field. Recompression and coalescence can then proceed. Earlier work [Winske, 1988] also included a background plasma; its absence makes little difference on the development of the instability.

The scaling of the wavelengths of the modes observed early ("linear") and later ("nonlinear") in the simulations can be checked with linear theory, as a function of the magnetic field strength and the ion to electron mass ratio. Figure 5 compares wavenumbers in terms of kc/ω_e normalized to R_B, versus the applied magnetic field (Ω_e/ω_e) [left panel] and m_i/m_e [right panel]. The squares correspond to measurements of k when the instability first appears, the circles to much later in the runs. The solid curves correspond to Eq. (6); good agreement with both Ω_e/ω_e and m_i/m_e scaling predicted by the equation is seen. Nonlinearly, there is very weak (if any) dependence on Ω_e/ω_e (as seen in the NRL experiments) and m_i/m_e.

As mentioned earlier, the instability has been observed in other kinds of simulations that have been carried out at LANL and elesewhere. Galvez et al. [1988] have only

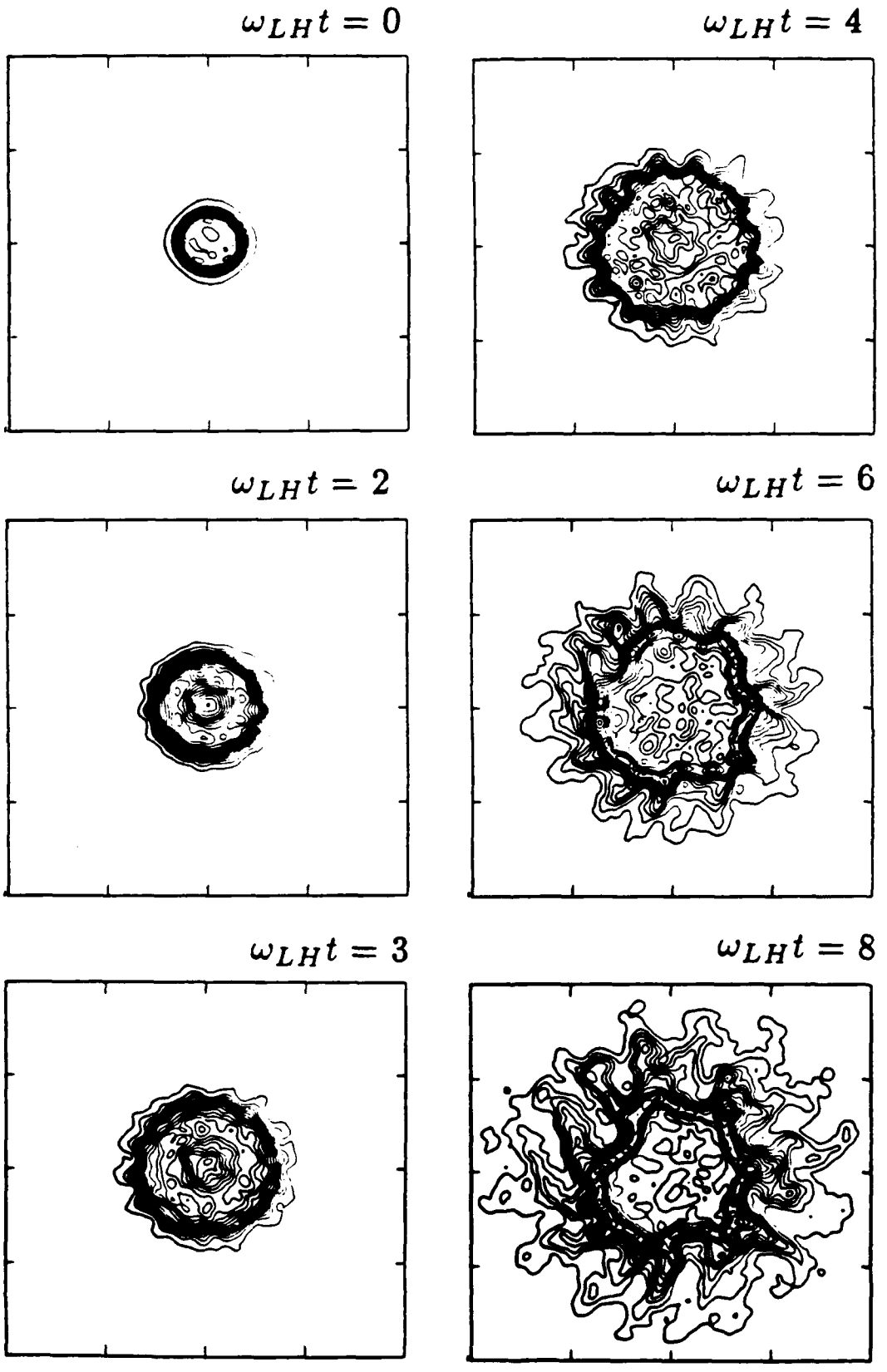

Figure 4. Results of 2-D electromagnetic particle simulations; ion density contours at various times showing shell formation and instability growth and evolution.

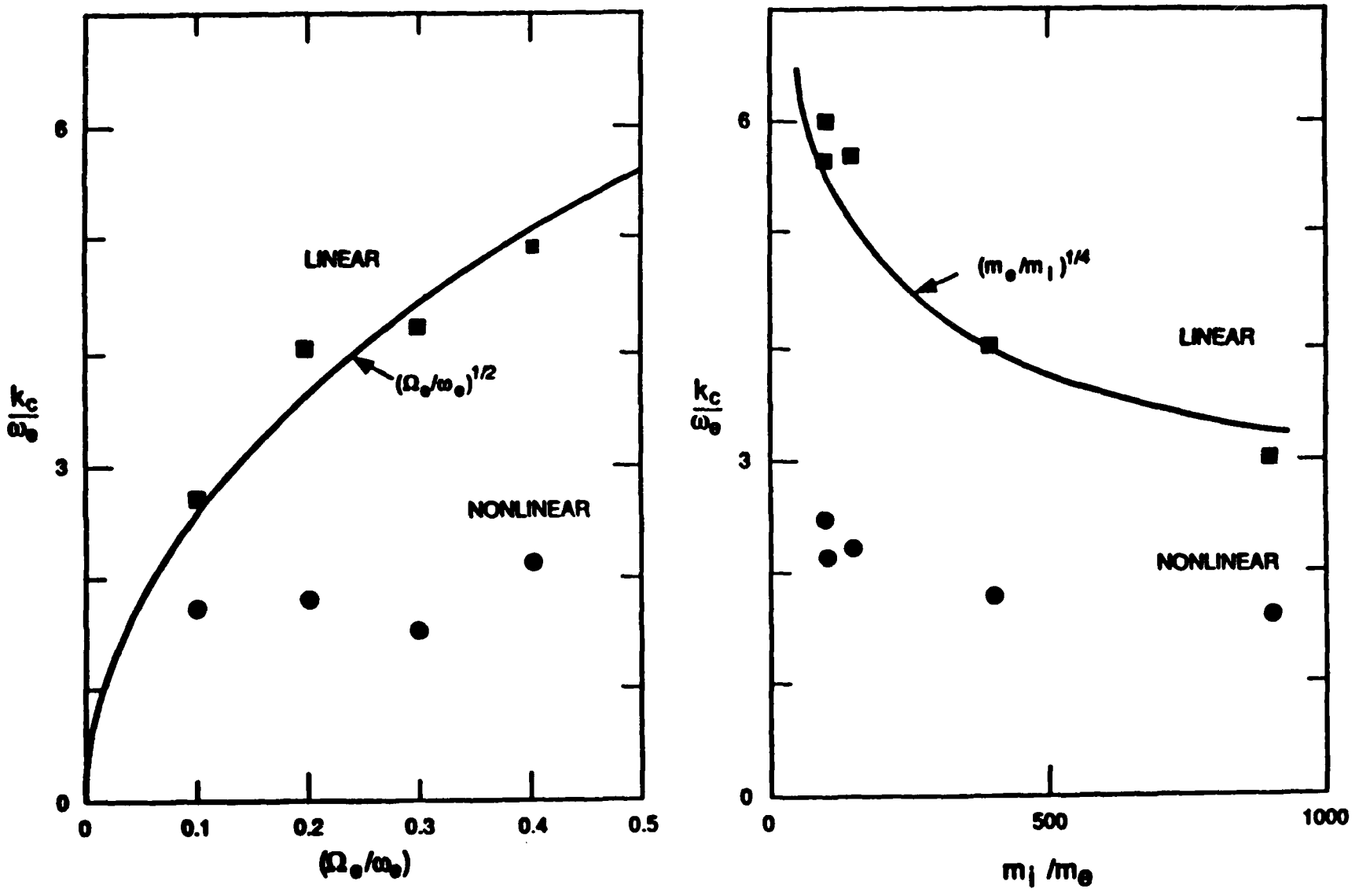

Figure 5. Results of a number of particle simulations showing wavenumber at early times ("linear", squares) and later on in the runs ("nonlinear", circles) versus magnetic field strength (Ω_e/ω_e) and ion mass (m_i/m_e); solid curves are Eq. (6).

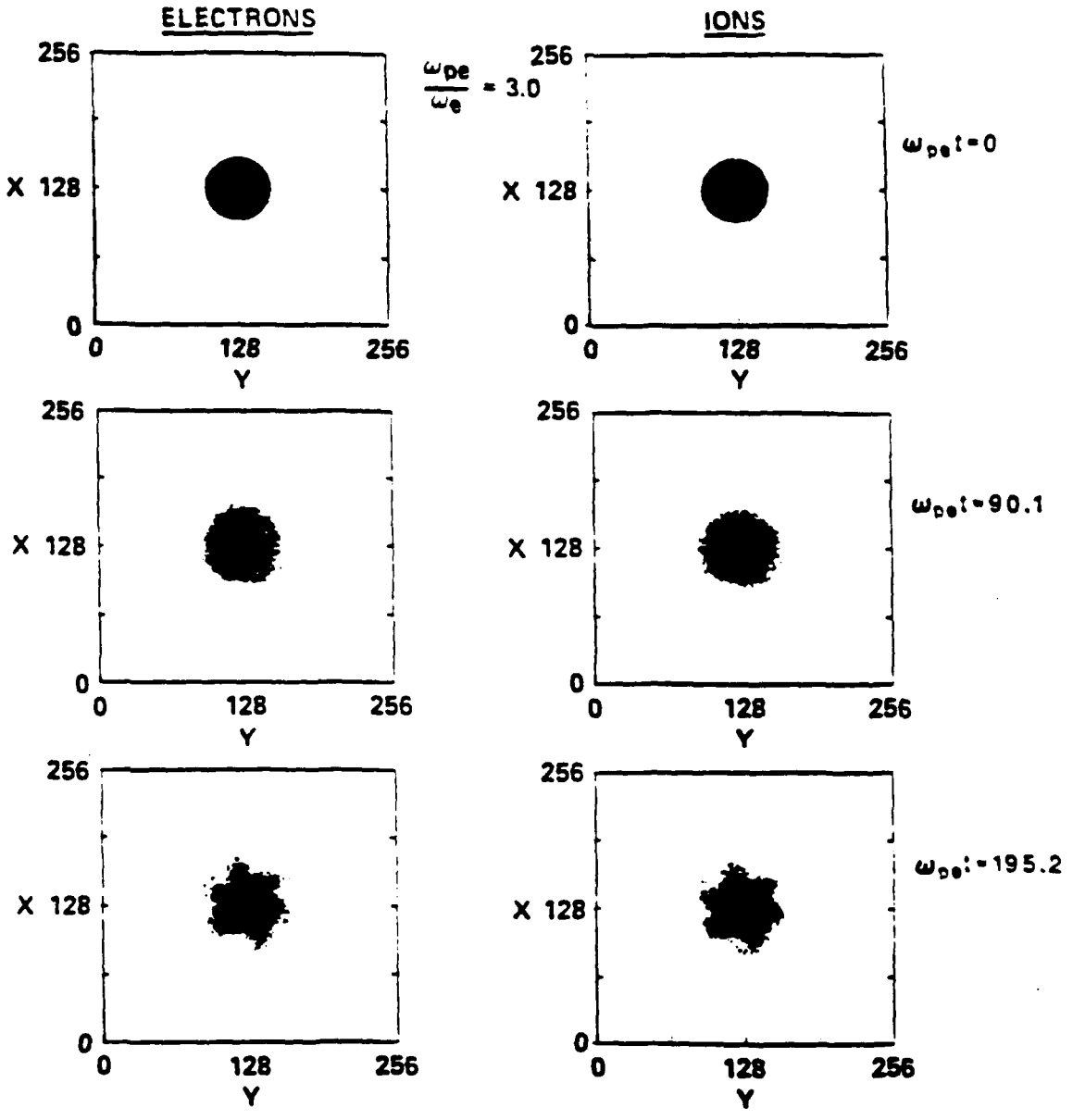

Figure 6. Results of 2-D electrostatic simulations showing electrons and ions in space at various times [from Galvez et al., 1988].

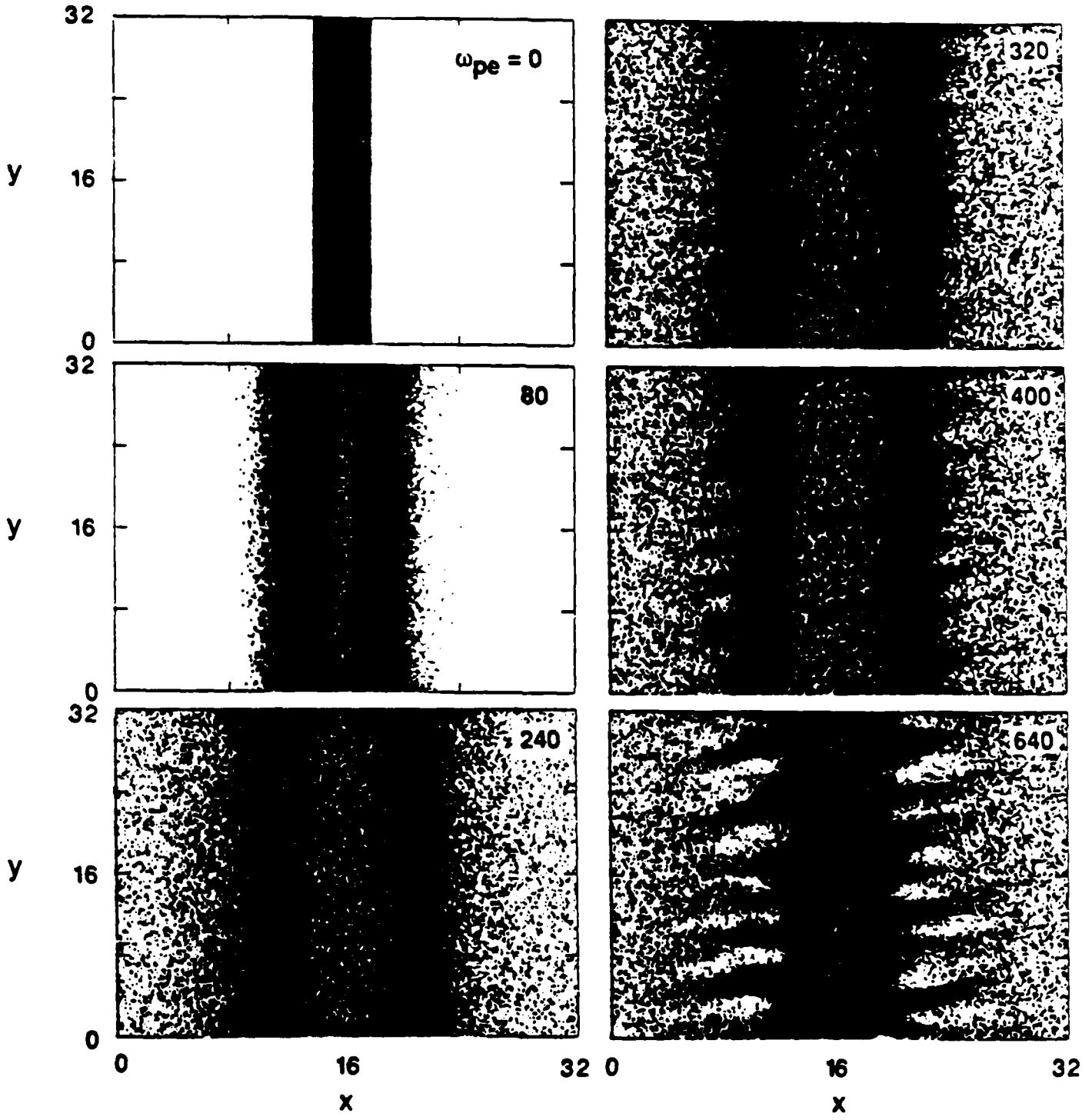

Figure 7. Results of 2-D hybrid simulations showing ions in space at various times [from Sgro et al., 1988].

electrostatic perturbations (i.e., no diamagnetic cavity forms), start with a large plasma $r_o \gg \rho_i$ and allow only a thermal expansion. In this case $V_g < V_n$, but the instability develops nevertheless. An example of such a calculation is shown in Figure 6, where the ions and electrons in configuration space are shown at various times. In constrast, Figure 7 displays the ions in x-y space for a plasma slab expanding against a magnetic field [Sgro et al., 1988]. The calculations were carried out using a hybrid (fluid electrons with $m_e \neq 0$, particle ions), again stressing that the instability persists without kinetic electron effects and that it does not depend on the plasma having a cylindrical shape.

3. Recent Enhancements to the Theory

This section treats a number of improvements to the basic theory and further simulation studies of early time structuring. The discussion is divided into nine subsections: (A) dynamics of the plasma expansion, (B) progess on a nonlocal theory, (C) linear theory with finite β_e, (D) ρ_i/R_B scaling, (E) mode coalescence, (F) asymmetric expansions, (G) 3-D simulations, (H) weak instability limit, and (I) collisions with the background plasma. We treat each of these topics in turn, with further discussion of their implications for the observations in Section 4.

A. Dynamics of Plasma Expansion

The standard approach to determine the maximum cavity size and deceleration is to consider the pressure balance relation:

$$\frac{1}{2}Nm_iV_D^2 \;=\; \frac{1}{2}Nm_iv^2 \;+\; \frac{B_o^2}{8\pi}\,V \tag{7}$$

where N is the number of debris ions, V_D is their expansion velocity, $v = dr/dt$, and where in 2-D $V = \pi r^2 L$ while $V = 4\pi r^3/3$ in 3-D, and take a time derivative to obtain $g = -dv/dt$. At maximum expansion ($v = 0$)

$$g_{\max} \;=\; a\frac{V^2}{R_B} \tag{8}$$

where $a = 1$ for 2-D and $a = 3/2$ for 3-D, while R_B is obtained by evaluating (7) at $r = R_B$. Expressing in terms of $V_g = g/\Omega_i$ and $v_A =$ Alfven speed assuming the debris ions are spread to uniform density [$N = n_B V(R_B)$], i.e., $v_A^2 = B_o^2/4\pi n_B m_i = V_D^2$ at $r = R_B$, one finds

$$V_g/v_A \;=\; a\rho_i/R_B \tag{9}$$

While the 2-D calculations, which assume the magnetic field is always transverse to the expansion, makes sense physically, the corresponding 3-D version is obviously a simplified

extrapolation that is valid only to some degree. More correct is to assume that the plasma expands along the magnetic field unimpeded by B, as simulations in which motion along B is included show [Gisler, 1988]. One can obtain a time dependent version of (7) for a better description of the dynamics, taking $V = \pi r^2(t)L(t)$ with $L(t) = L_o + V_D t$ [Gisler and Lemons, 1988]. In this case the solution is more complicated and involves Airy functions. One finds from the solutions that the time of maximum deceleration is slightly greater than the time of maximum extent (R_M), with

$$(V_g/v_A)_{\max} = a\rho_i/R_B \tag{10}$$

with $a \simeq 2.3$ and

$$(R_M/R_B)_{\max} = 0.88 \tag{11}$$

with R_B defined using (7).

Thus, the effective deceleration is some 50% larger than expected from the more simple minded 3-D model. Using a larger g in the linear theory, of course, gives maximum growth rates that are larger and occur at somewhat longer wavelength (cf. Figure 3).

B. Nonlocal Theory

We have also carried out a nonlocal analysis of the lower hybrid drift instability in order to compare with the local theory. The calculations are done in the electrostatic limit with cold electrons and ions. As before, the electrons are subject to an $\vec{E} \times \vec{B}$ drift, V_E, on the surface. Now, however, we make no assumptions about the frequency ω and we assume a sharp boundary density profile: $n(x) = n_o,\ x < b,\ n(x) = 0,\ x > b$, while the electrostatic potential $\delta\phi \sim \delta\phi(x)e^{iky-\omega t}$. The details are found in Lemons [in preparation, 1988]; here we merely summarize the major results and conclusions.

With this model one can, as before, carry out a local analysis at $\delta\phi(b)$, obtaining the dispersion equation

$$1 + \frac{\omega_e^2}{\Omega_e^2(1-\bar{\omega}^2/\Omega_e^2)} + \frac{\epsilon_n\omega_e^2}{k\Omega_e\bar{\omega}(1-\bar{\omega}^2/\Omega_e^2)} - \frac{\omega_i^2}{\omega^2} = 0 \tag{12}$$

where $\bar{\omega} = \omega - kV_E$. If one assumes $\bar{\omega}/\Omega_e \ll 1$, one obtains the usual lower hybrid drift instability dispersion equation in the electrostatic (fluid) limit.

To do a nonlocal theory requires matching solutions for $\delta\phi(x)$ for $x < b$ and $x > b$ at $x = b$. This is done by integrating Poisson's equation from $b - \epsilon$ to $b + \epsilon$ and letting $\epsilon \to 0$, assuming $\delta\phi$ is continuous, and obtaining

$$2 + \frac{\omega_e^2}{\Omega_e^2(1-\bar{\omega}^2/\Omega_e^2)} + \frac{\omega_e^2}{\Omega_e\bar{\omega}(1-\bar{\omega}^2/\Omega_e^2)} - \frac{\omega_i^2}{\omega^2} = 0 \tag{13}$$

At this point one needs to be careful not to throw out the $\bar{\omega}^2/\Omega_e^2$ terms right away, but instead combine the second and third terms, obtaining

$$2 + \frac{\omega_e^2}{\Omega_e \bar{\omega}(1 - \bar{\omega}/\Omega_e)} - \frac{\omega_i^2}{\omega^2} = 0 \tag{14}$$

In this form Eq. (14) looks like the local equation (12) except that $1 + \omega_e^2/\Omega_e^2 \rightarrow 2$ and $\epsilon_n/k \rightarrow 1$ in the third term. (If one throws out the $\bar{\omega}^2/\Omega_e^2$ terms in (13) first, the first term becomes $2 + \omega_e^2/\Omega_e^2$.) In the long wavelength ($k \rightarrow 0$) limit these differences do not matter, as one neglects these terms regardless and solves the remaining quadratic equation to obtain

$$\omega \simeq \frac{\Omega_i}{2} + i(kV_E\Omega_i)^{1/2} \tag{15}$$

in agreement with earlier work [Peter et al., 1983], but contrary to Hassam and Huba [1987]. In this form the growth rate looks like that of a Rayleigh-Taylor instability. $\gamma \sim k^{1/2}$. It is also interesting to note that in the high frequency limit $\bar{\omega}/\Omega_e > 1$, one does not obtain maximum growth due to the lower hybrid drift instability from (14), rather the much shorter wavelength Buneman instability dominates, $\omega \sim \omega_e(m_e/2m_i)^{1/3}(1 + i\sqrt{3})/2$. On the other hand, if one throws out the $\bar{\omega}^2/\Omega_e^2$ terms in (13) from the start, one obtains a dispersion equation which looks like the local theory (12) [Batchelor and Davidson, 1976]. Numerical solutions obtained by Batchelor and Davidson [1976], which give the lower hybrid drift instability, however, are inconsistent in that $\bar{\omega}/\Omega_e$ is not small.

The conclusion from this analysis is that one has to be very careful in applying either the local or nonlocal theory to the problem. For short wavelength modes, where $k \sim \epsilon_n$, the local theory is most appropriate. The nonlocal analysis can give inconsistent results: it either gives maximum growth at frequencies much higher than the lower hybrid frequency, yielding solutions at wavelengths much shorter than the density scale length or gives roots that violate $\bar{\omega}/\Omega_e < 1$. Such short wavelength modes are quite sensitive to the very unrealistic sharp boundary that has been assumed. On the other hand, for the long wavelength modes the sharp boundary approximation is valid, as the broad radial eigenfunctions experience the boundary only in an average sense, while the local approximation in this regime is likely to be less accurate. Thus, in this limit Eq. (15) is a better approximation to the growth rate than is the $\gamma \sim k$ scaling of Hassam and Huba [1987].

C. Finite β_e Effects

The linear analysis in Winske [1988] has been improved to include finite electron temperature effects. The addition of such effects is a straightforward, but tedious procedure [Davidson et al., 1977, Zhou et al., 1983]. The method followed here is that of Zhou et al. [1983], where the dispersion equation is derived in some detail. An example of how such effects change the linear properties is found in Figure 8, where the growth rate is plotted versus wavenumber for two values of T_e. The parameters are the same as in Figure 3; the curves are drawn on the same scale for easy comparison. At low values

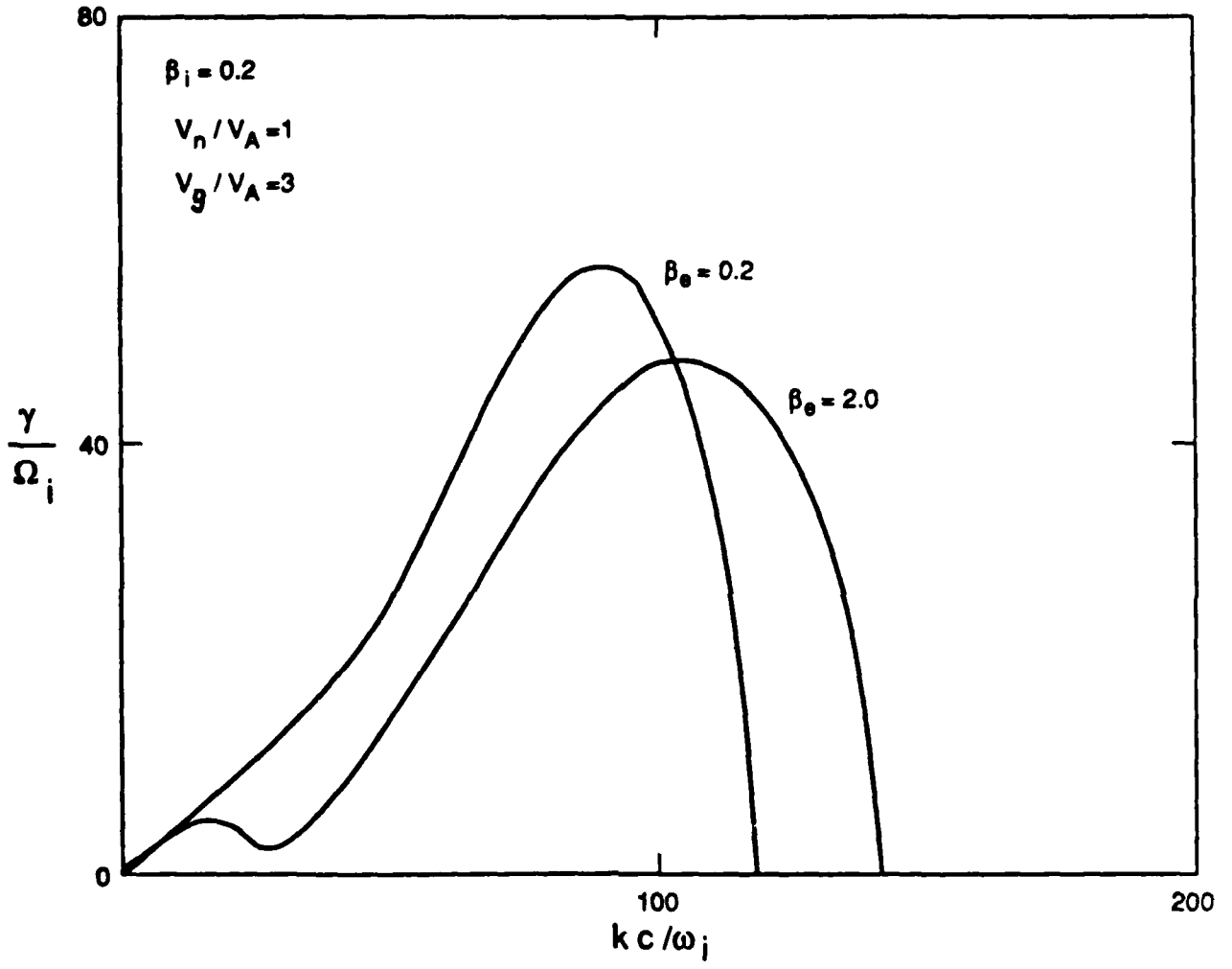

Figure 8. Growth rates versus wavenumber for the lower hybrid drift instability with deceleration including finite β_e effects (Parameters same as Figure 3).

of T_e ($\beta_e = 0.2, T_e = T_i$ in the figure), the inclusion of finite electron temperature has three effects. First, because V_E is increased, the maximum growth rate is slightly larger. Second, because of finite T_e, k corresponding to maximum growth increases slightly. Third, at small k, there is an enhancement in the growth rate for $V_g \neq 0$ at modest β_e. At higher β_e, this enhancement at small k disappears, the wavenumber at maximum growth increases slightly, but the overall growth rates are reduced.

The fact that k increases with β_e may seem contrary to Figure 21 of Winske [1988], which shows k at maximum growth decreasing with β. There, however, T_i was also changing to keep $T_i = T_e$, and the decrease in k was primarily due to an increase in T_i. However, for sufficiently large β_e the short wavelength modes are suppressed [Drake et al., 1983], as also shown in Figure 21 of Winske [1988]. This effect is due to strong damping of the electrons by the magnetic field gradient. One can easily show from Ampere's law that $\nabla B/B \sim \beta_e^{1/2}(V_E/v_e)\omega_e/c$. The bottom line is that finite β_e effects play a minor role and can be neglected in favor of the simpler $T_e = 0$ dispersion equation, unless $\beta_e \gg 1$.

D. ρ_i/R_B Scaling

As mentioned in the Introduction, various experiments suggest that ρ_i/R_B = ion gyroradius/magnetic confinement radius is an important parameter. The structures that appear on the surface of expanding plasmas are larger and more prominent for $\rho_i/R_B > 1$, as occur in the NRL laser experiment [Ripin et al., 1987]. Zakharov et al. [1986] suggest that strong cross-field diffusion occurs in this limit, as discussed later in this subsection. Furthermore, plasmoid propagation studies show that $\rho_i/R_B \sim 1$ (where R_B is now the plasma radius) separates different physics regimes [Papadopoulos et al., 1988; Wessel et al., 1988]. Again, for $\rho_i/R_B > 1$, i.e., when the ions are essentially unmagnetized, anomalous effects allow the plasmoid to propagate more effectively across the magnetic field.

Figure 9 shows the results of a number of 2-D electromagnetic particle simulations where ρ_i/R_B was varied, by changing m_i/m_e and Ω_e/ω_e, keeping the magnetic confinement radius $R_B \sim (m_i/m_e)^{1/2}\omega_e/\Omega_e$ = constant (in 2-D) [note $\rho_i \sim (m_i/m_e)\omega_e/\Omega_e$]. In each case the simulations are shown at the same instant of time $\omega_{LH}t = 8$; contours of the ion density are plotted. A number of features are clearly evident. For large ρ_i/R_B the plasma compresses into a thinner shell, the instability appears to develop quicker, and the modes have longer wavelength. In the first two cases, indeed the instability develops so rapidly that one sees the nonlinear, coalesced structures. And in the smallest ρ_i/R_B case, the plasma has not yet reached its maximum expansion. In addition, for larger ρ_i/R_B the final size of the plasma is smaller, the ions are better confined, recompression of the central core is more evident, and coalescence to longer wavelengths is more likely. A number of these effects can be inferred from linear theory. For example, because $\rho_i/R_B \sim V_g/v_A$, the deceleration is more rapid and as a consequence, compression into a thinner shell results. In addition, larger V_g/v_A implies a larger growth rate and longer wavelengths (Figure 3). Figure 10 reconfirms this, by comparing the observed k's in the linear (early time) and nonlinear (later time) regimes as a function of ρ_i/R_B with linear theory. Overall, there is

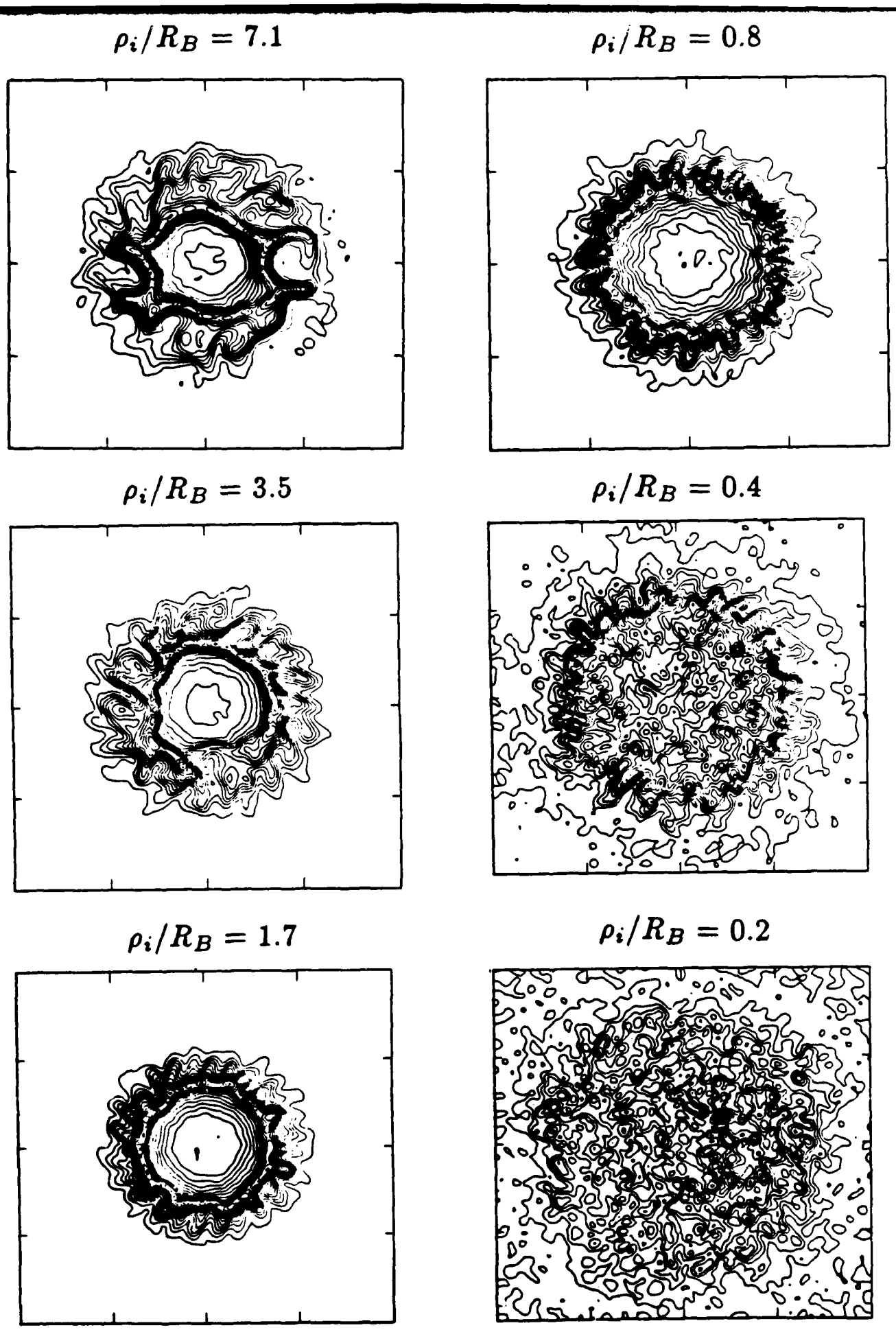

Figure 9. Results of 2-D particle simulations showing ion contour plots at one time ($\omega_{LH}t$ = 8) for several runs in which R_B =constant, but ρ_i/R_B is varied.

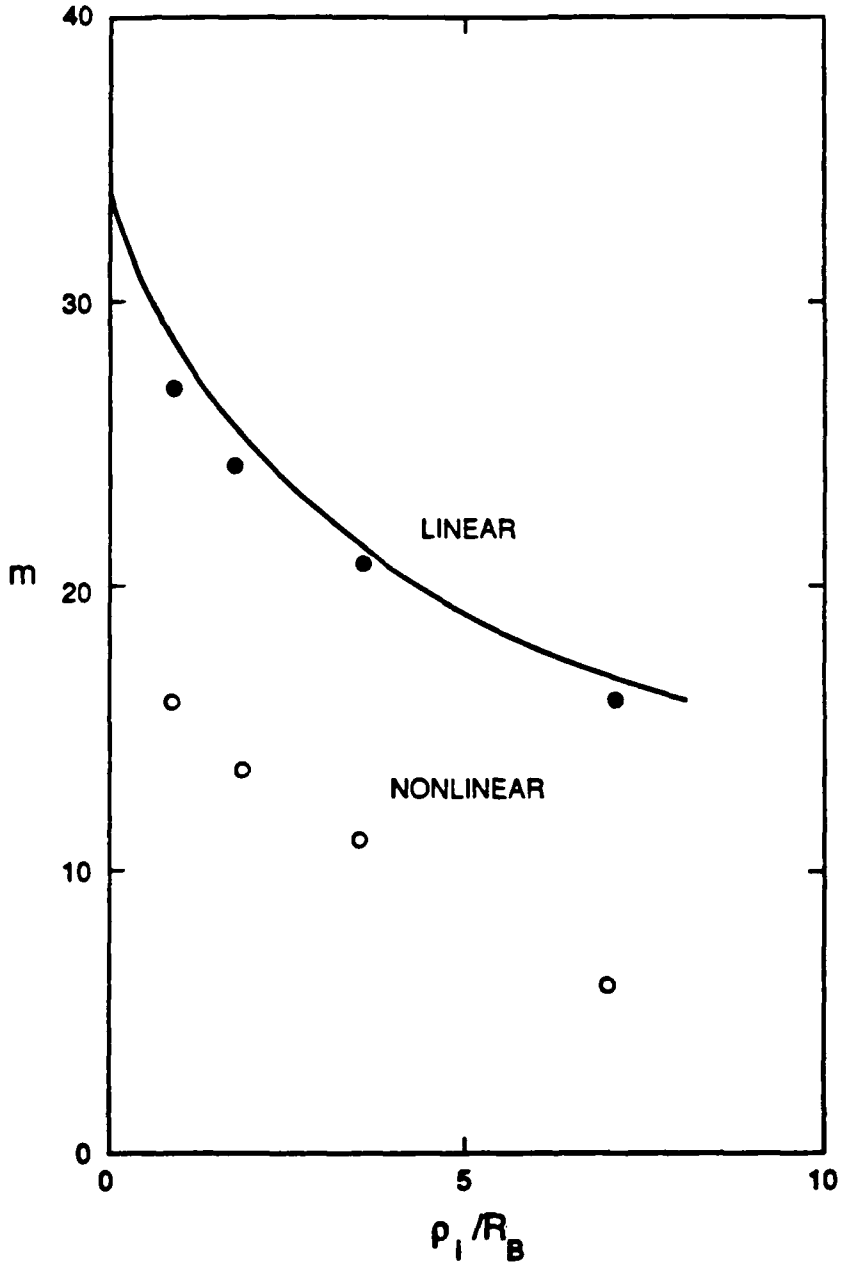

Figure 10. Results from linear theory (solid line) showing wavenumber at maximum growth versus ρ_i/R_B; closed circles (open circles) correspond to the simulation results at early (late) times.

a good match; the nonlinear k's suggest stronger coalescence at larger ρ_i/R_B. While the stronger (i.e., larger free energy) expected at larger ρ_i/R_B also explains the larger size of the structures, the fact that the final radius of the bulk of the plasma is smaller is less intuitively obvious.

The results, however, are consistent with the experiments of Zakharov et al. [1986], who argue as follows. The plasma radius as a function of time consists of two terms, one due to expansion, the other due to diffusion of the plasma through the field:

$$r(t) = V_D t - Ct^2 \tag{16}$$

The diffusion is so strong that the final radius $R_M < R_B$ so that the expansion goes just as $V_D t$ rather than as $R_B \sin(V_D t/R_B)$ [Winske (1988)]. Here, $Ct^2 = (Dt)^{1/2}$, where D is the diffusion coefficient ($D = \nu c^2/\omega_e^2$) and ν = anomalous collision frequency = $\varsigma\omega_{LH}$ with ς = constant. The plasma reaches its maximum radius R_M when $dr/dt = 0$, i.e., at $t_M = V_D/2C$ and

$$R_M = \frac{V_D^2}{4C} = \frac{R_B}{4(\varsigma\rho_i/R_B)^{1/2}} \tag{17}$$

Figure 11 plots R_M/R_B, as measured in the simulations, versus ρ_i/R_B. Qualitatively consistent with Zakharov et al. [1986], when $\rho_i/R_B < 1$, $R_M/R_B \sim 1$ (in practice this is used to more accurately determine R_B when thermal effects are included). On the other hand, when $\rho_i/R_B > 1$, $R_M < R_B$; a straight line through the points gives $R_M/R_B \sim (\rho_i/R_B)^{-0.3}$, which is a weaker dependence than Eq. (17). The derivation of (16), however, assumes a 3-D expansion so that $N \sim nr(t)^3 \sim n(t)(V_D t)^3$ and a constant resistivity. In fact, the simulations are 2-D, which implies $N \sim t^2$. In this case Eq. (17) is slightly less elegant, because the last term $\sim t^{3/2}$; the same method of solution now yields $R_M/R_B \sim (\rho_i/R_B)^{-1}$. Better agreement occurs assuming that $N \sim t^2$ but $\varsigma \sim t^2$ (i.e., the waves grow in time and hence the anomalous collision frequency increases in time); then $R_M/R_B \sim (\rho_i/R_B)^{-1/3}$. Alternatively, one can argue that, consistent with the usual lower hybrid drift instability [Winske and Liewer, 1978], ν is not constant but varies as $(\rho_i/R_B)^{-1/3}$, then (17) yields $R_M/R_B \sim (\rho_i/R_B)^{-1/3}$. None of these fixes is entirely satisfactory. However, the basic idea that when the instability is strong, diffusion of the plasma by the waves eventually limits the cavity size (R_M) to be less than the classical limit (R_B) seems physically reasonable and supported by the simulations.

Two other additional points should be made. First, one can estimate when the diffusion picture should break down. The usual plasma expansion model (Sec. 3A) shows that

$$r(t) \sim R_B \sin(V_D t/R_B) \sim V_D t - (V_D t)^3/3R_B^2 \tag{18}$$

We have ignored the second term in favor of a diffusion term $\sim Ct^2$. Obviously, if the collision frequency is too small, the t^3 dynamic correction term in (18) determines the radius, not the diffusion. Again, one can show that diffusion dominates for $\rho_i > R_B$.

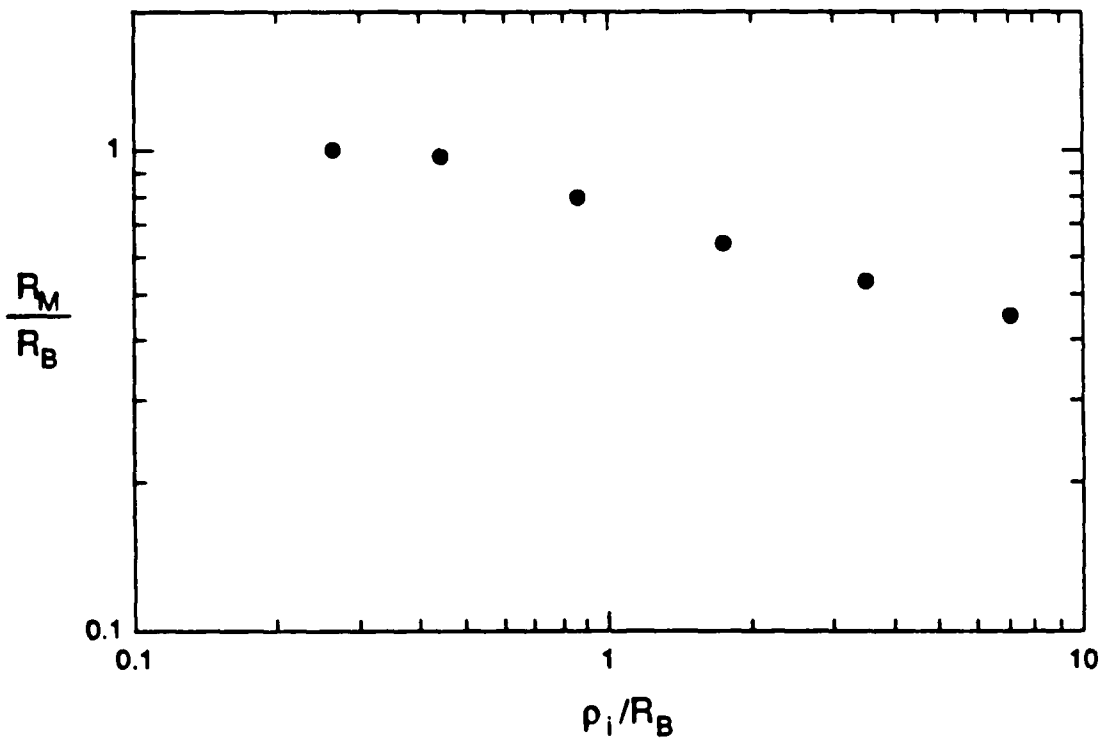

Figure 11. Results of simulations showing R_M/R_B versus ρ_i/R_B.

Second, even though the magnetic field cavity grows to maximal size, the outer edges of the plasma continue to expand outward. This is already somewhat evident from the simulation shown in Figure 4. To see the magnetic cavity for this case in more detail and its relation to the position of the plasma, Figure 12 displays cuts in x through the center of the simulation region, showing the ion density and the magnetic field B_z at various times. One sees that a well defined cavity forms at early times, the plasma compresses into a thin shell, and the cavity and plasma are of comparable size. At later time, the cavity starts to collapse along with the inner portion of the plasma, while the other edge of the plasma remains moving outward. This corresponds to the freestreaming of the flutes seen in the NRL experiment [Ripin et al., 1987].

E. Mode Coalescence and Nonlinear Effects

The simulation shown in Figure 4 as well as the larger ρ_i/R_B cases in Figure 9 indicate that longer wavelength modes prevail at late times. Several explanations for this effect are possible. First, because the longer wavelength modes have smaller linear growth rates, they will take longer to grow to large amplitude. Second, because the longer wavelength modes appear during or slightly after maximum expansion, when the deceleration is larger, the longer wavelengths may be a linear consequence of a larger effective g (cf. Figures 3 and 10). Third, the longer wavelength modes may result from nonlinear coupling of the shorter wavelength modes. It is known, for example, that the wavelengths associated with the lower hybrid drift instability in the post implosion phase of a theta pinch are typically about a factor of two longer than those calculated from linear theory at maximum growth [Fahrbach et al., 1981]. Drake et al. [1984] have constructed a mode coupling theory whose numerical solutions give quantitative agreement with those observations. The theory is based on the idea that when the waves grow to sufficient amplitude, the nonlinearity allows the frequency mismatch to be overcome and coupling of the pump wave at wavenumber k_o to daughter waves at $k \sim k_o/2$ can proceed. Although the theory has been constructed in the weak drift regime with $V_g = 0$, which is not directly applicable to our situation, the physics of the decay may persist anyway.

Figure 13 displays the results of a number of simulations run with various parameters showing the amount of coalescence, as determined by the ratio of the mode number observed during the linear growth phase (m_L) to that observed in the later phase (m_{NL}), versus ρ_i/R_B. Several points can be inferred from the plot. First, the amount of coalescence for all of the runs is between two and three, with an average value of 2.5. Second, there is no strong variation with ρ_i/R_B. Third, there is considerable scatter in the data, which in part reflects the difficulty in determining m_L and m_{NL}, and also the fact that the parameters vary over a wide range. The wide scatter may obscure any weak scaling, and may also suggest that ρ_i/R_B is not the best parameter to characterize the coalescence. The overall results, however, seem in qualitative agreement with the Drake et al. [1984] theory.

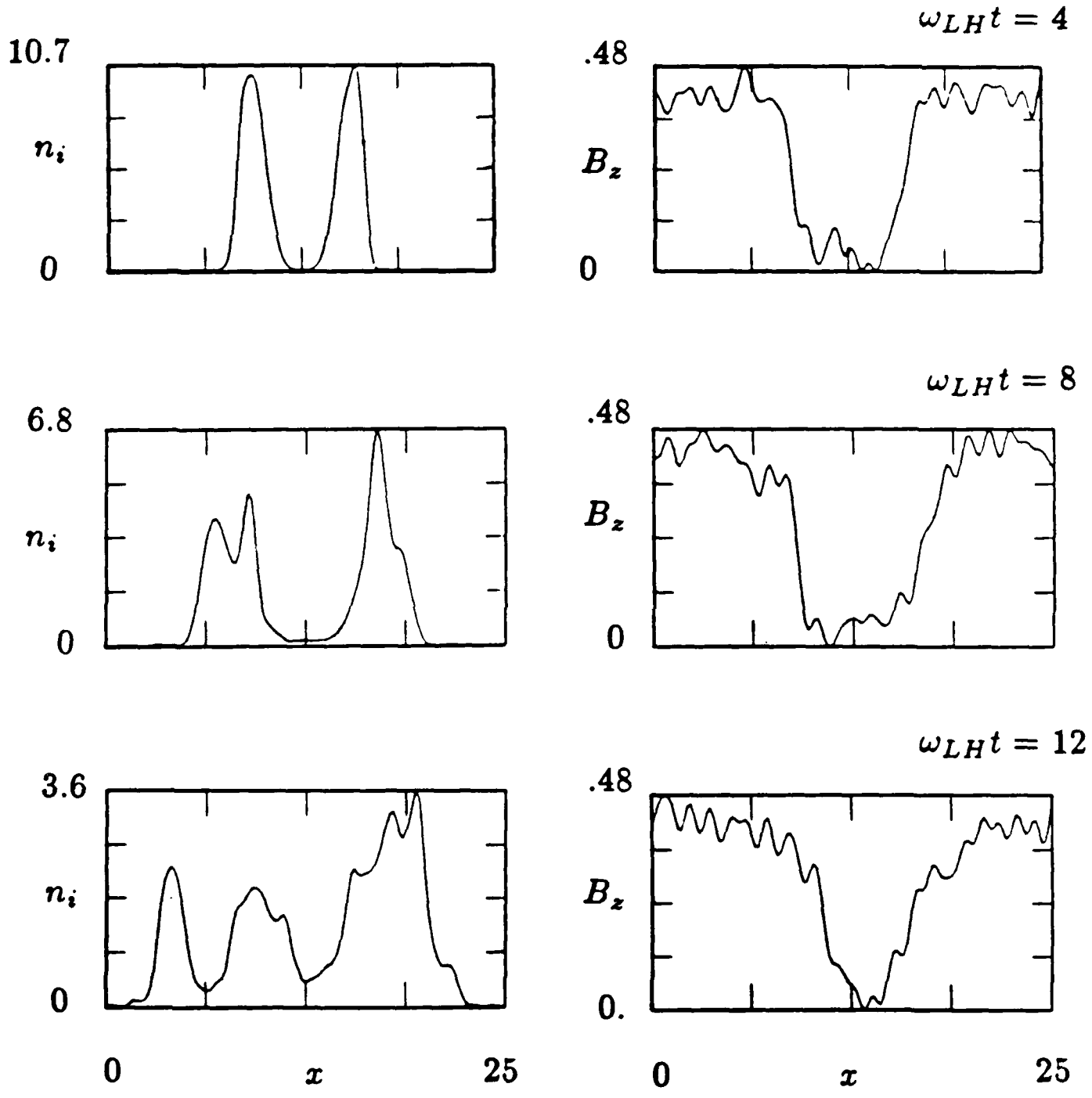

Figure 12. Cuts through x of the simulation of Figure 4, showing the ion density profile and the diamagnetic cavity at various times.

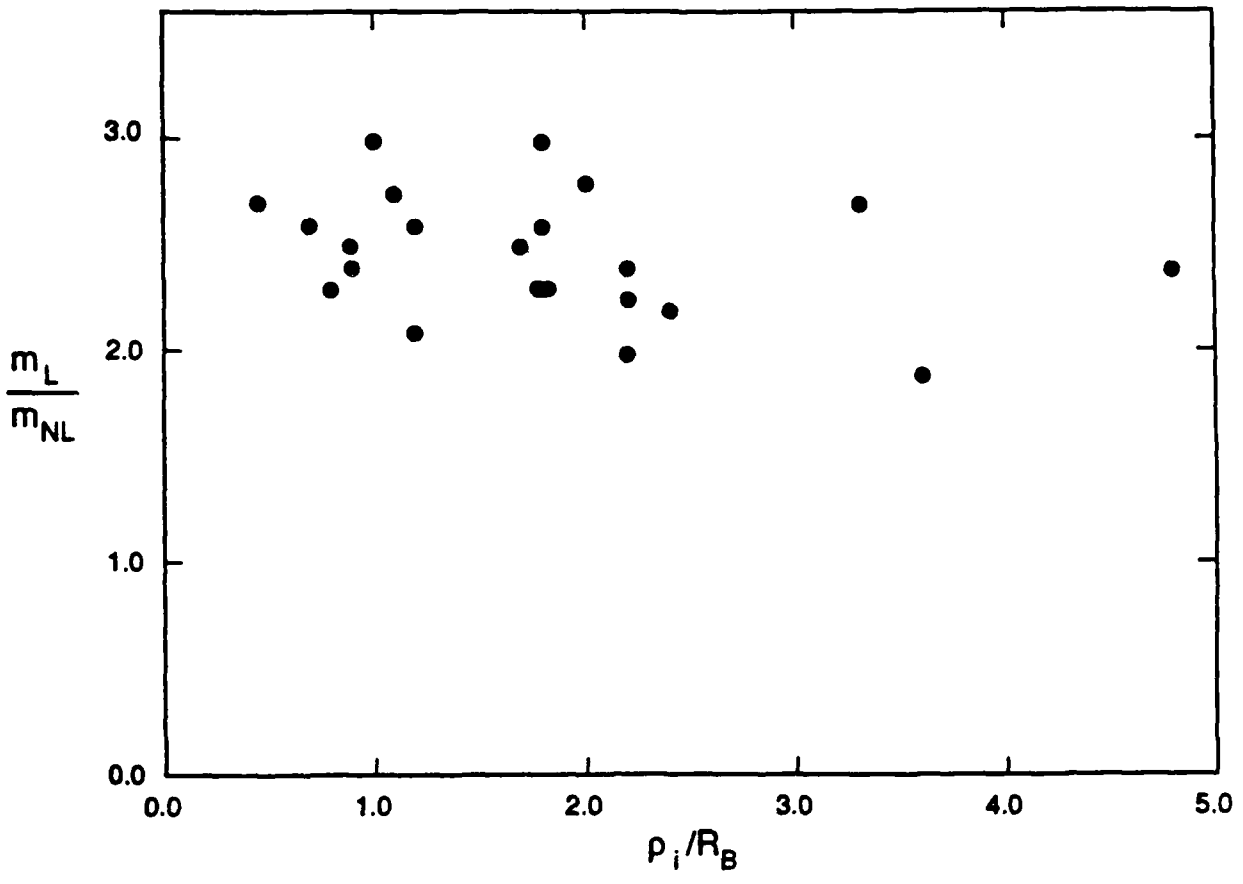

Figure 13. Results of a number of 2-D electromagnetic particle simulations showing the ratio of the mode number observed in the linear stage (m_L) to that in the nonlinear stage (m_{NL}) versus ρ_i/R_B.

In order to investigate the coalescence question further, two additional studies have been carried out. First, we have rezoned the calculations to allow them to run longer. Figure 14 shows the run displayed in Figure 4, run to longer times ($\omega_{LH}t = 16$) in a bigger mesh ($L_x, L_y \rightarrow 40c/\omega_e$). Three points should be noted. First, after the initial coalescence by about a factor of two, there is no further merging of the modes. Second, while the central core of the plasma collapses (along with the magnetic cavity), the outer parts of the plasma continue to expand, as was noted in the previous section. Third, the tips of the larger structures appear to bifurcate. This may be another nonlinear effect, or more likely, is the reappearance of the original, shorter wavelength modes [Winske, 1987].

We have also carried out a detailed study of the mode structure for a selected number of runs. To show the propagation of the waves in more detail, Figure 15 plots the density perturbations as a function of θ at the front edge of the expanding plasma shown in Figure 4 at various times. The average value of n_i has been subtracted out and the amplitudes have been normalized to unity. At early times, one sees the appearance of the short wavelength modes which move slowly, but perceptively in the positive θ direction (the direction of the electron drift). Although the phase velocities of these waves are small, the fact that k is large (mode $\sim$ 17 dominates) allows ω_r to be appreciable. In fact, from measuring the phase speed of several of the perturbations, one finds $\omega_r \sim 1.5\omega_{LH}$, in agreement with linear theory. At later times, these shorter wavelength modes merge into longer wavelength structures with much lower phase velocities and $\omega_r \sim 0$.

To show the properties of the waves in more detail, Figure 16 displays the Fourier spectra of the density perturbations $|n_k|^2$, k=1,2,...40 at various times. The spectra are determined from Fourier analyzing the density fluctuations every $0.25\omega_{LH}^{-1}$ and then averaging the spectrum over several intervals. At early times ($\omega_{LH}t = 2 - 3$) we see the emergence of short wavelengths (modes m=13-17), which shift to slightly higher mode number in the next frames. At later times, longer wavelength modes (m=7-8) then grow up and dominate. This can be seen more clearly in the next picture, Figure 17, where the Fourier modes are plotted versus time. Again, the growth of shorter wavelength modes is evident for $\omega_{LH}t < 5$, with the longer modes dominating later. Note that there does not seem to be a cascade through a progression of modes down to m=7-8, as modes 9-12 do not ever grow appreciably. For comparison with linear theory, the solid curve denoted the maximum linear growth rate (which occurs at short wavelength), while the dashed curve is the predicted linear growth rate for modes 7-8. The results suggest that the late time growth of modes 7-8 is a nonlinear consequence, not a slower linear growth to larger amplitude.

Finally, another possible nonlinear effect should be mentioned. Sgro et al. [1988] observed no coalescence in their hybrid simulations with $m_i/m_e = 100$, but a coalescence by about a factor of two with $m_i/m_e = 1836$. While the results are consistent with those of Figure 13, Sgro et al. [1988] have suggested that the coalescence scales as $(m_i/m_e)^\alpha$ with $\alpha \sim 1/4$. (This is also consistent with Figure 5.) This scaling is consistent with their simulations and when scaled to the mass of barium ions ($m_{Ba}/m_p = 137$) also gives the correct wavelength for the structures observed in the AMPTE releases.

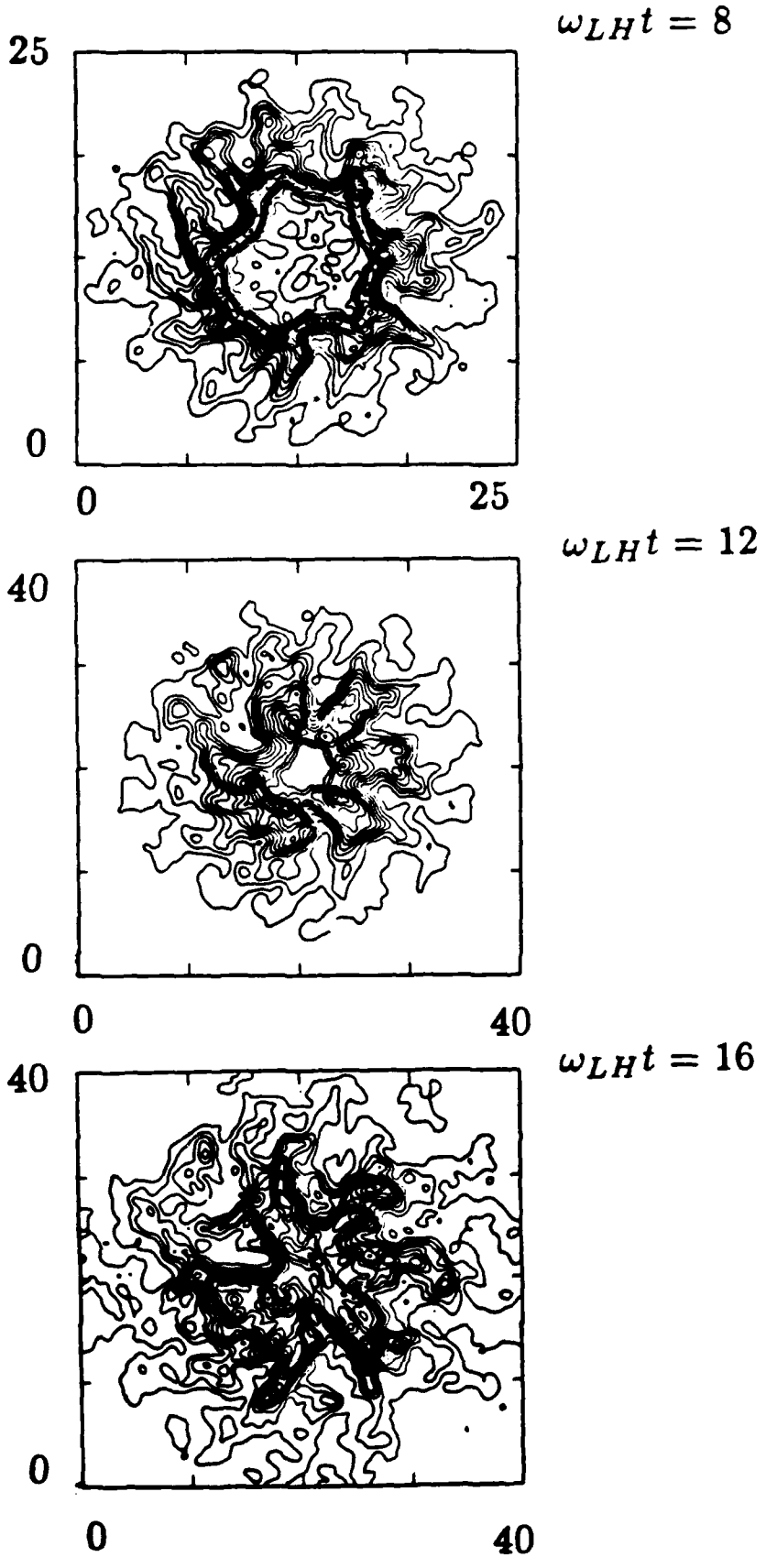

Figure 14. Ion density contours at various times for the same run as shown in Figure 4, extended to later time by expanding the simulation box.

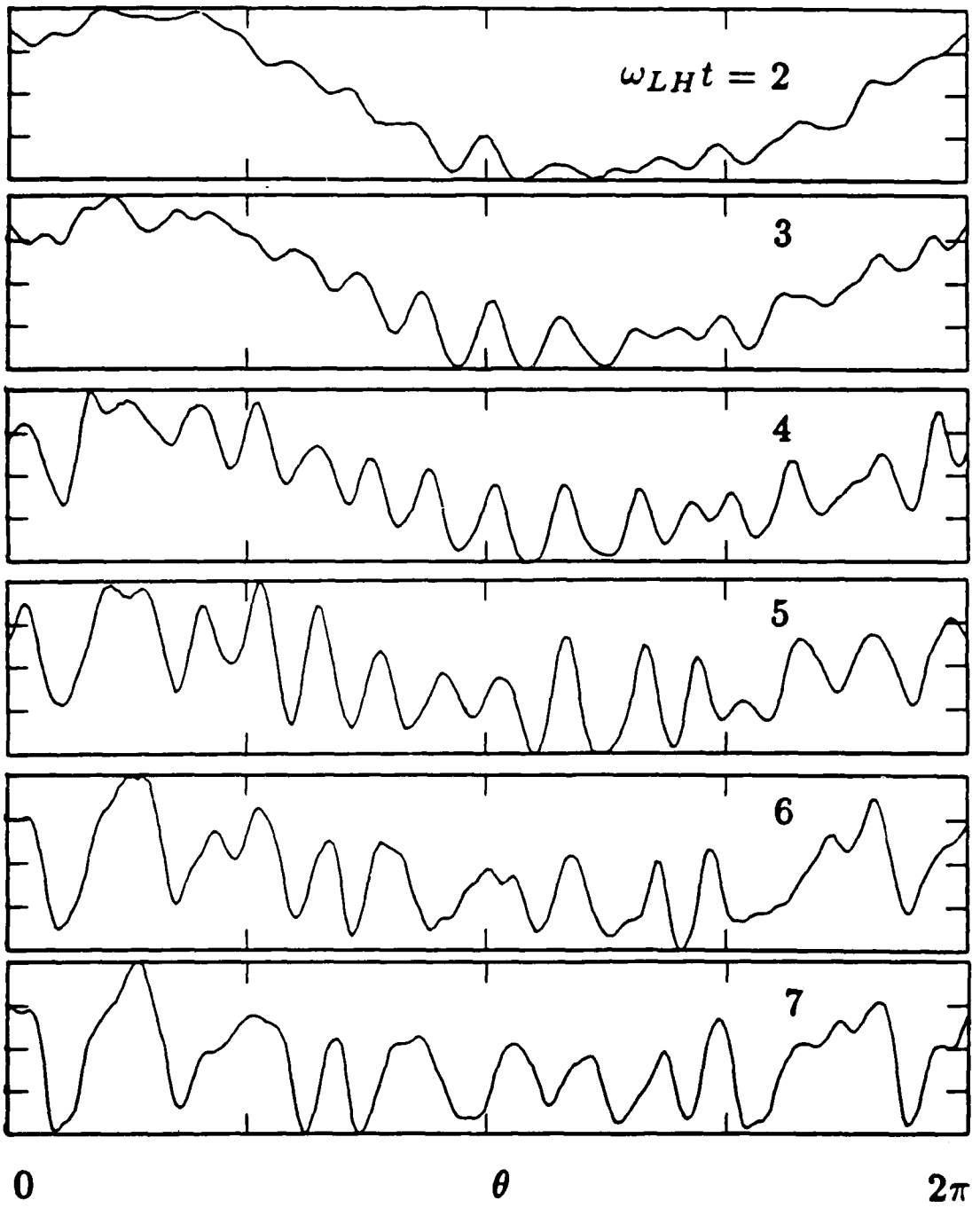

Figure 15. Density perturbations at the surface of the expanding plasma versus the azimuthal angle θ at various times for the run shown in Figure 4.

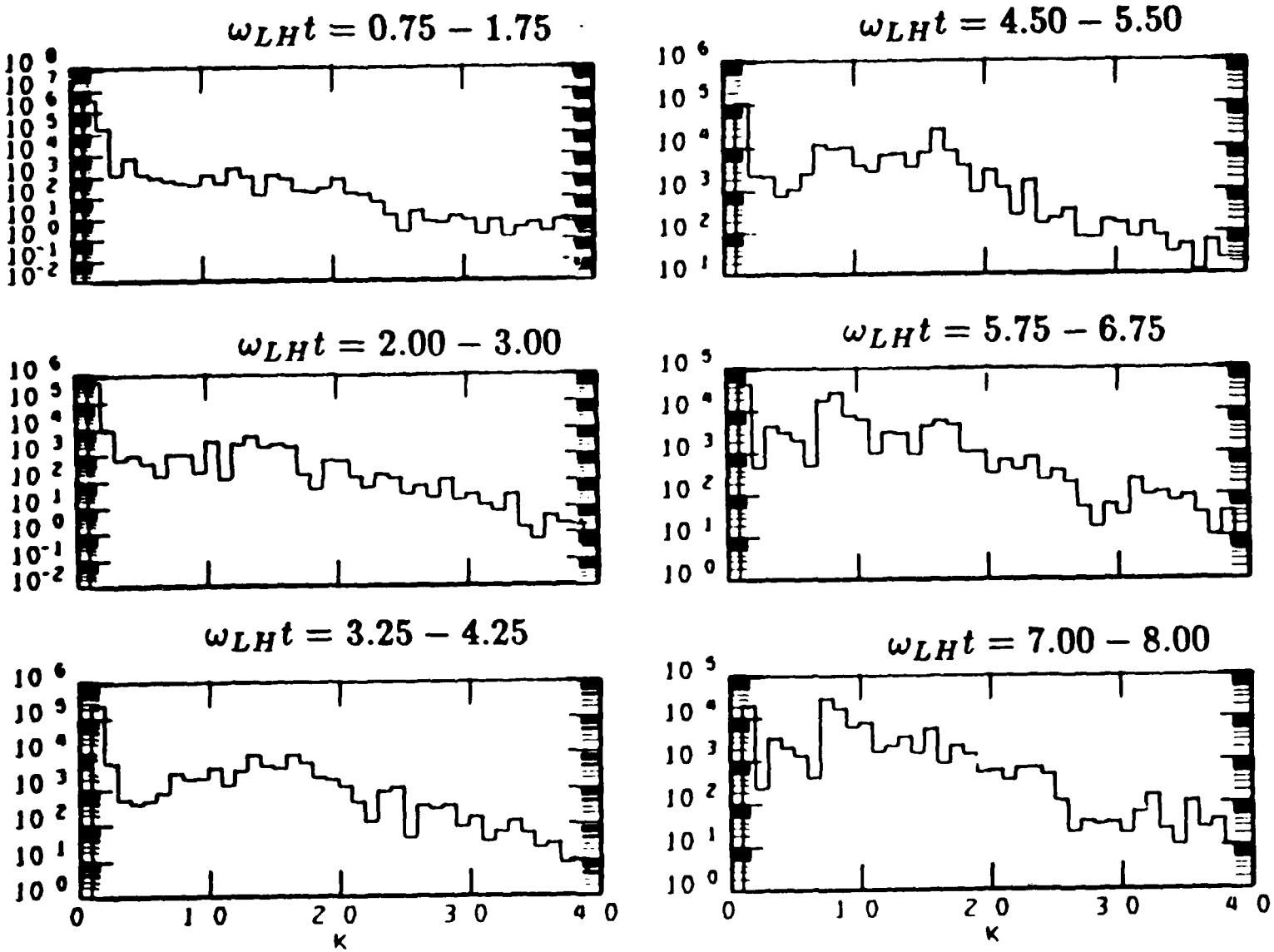

Figure 16. Fourier spectra of the density fluctuations averaged over various time intervals for the same run.

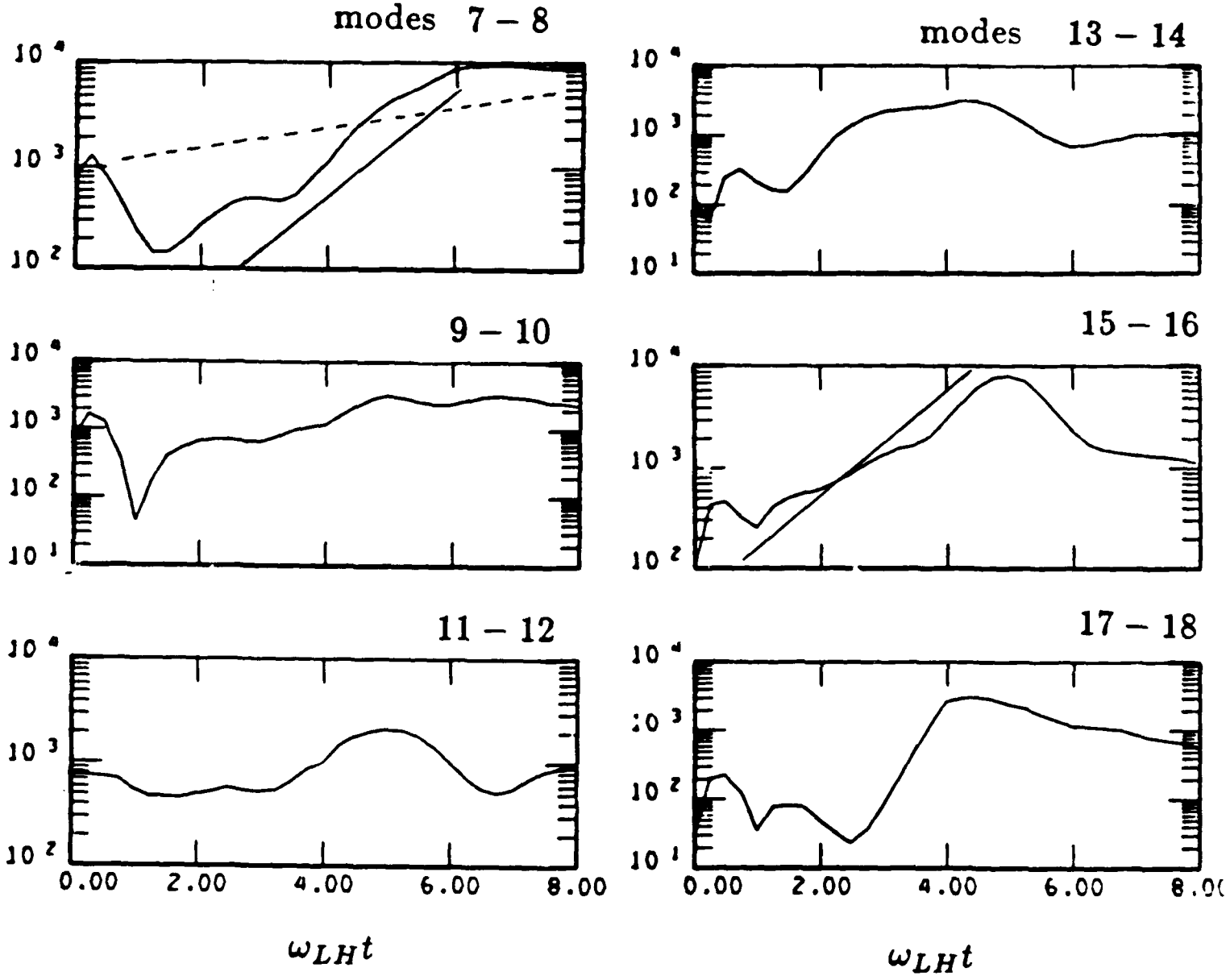

Figure 17. Time histories of the Fourier modes shown in the previous figure. Solid lines correspond to the maximum linear growth rate; dashed line is the linear growth rate for modes 7-8.

F. Asymmetric Expansions

While the perfectly symmetric expansions are convenient for theory and numerical simulations, one expects asymmetries to occur in laser initiated plasma expansions as well as in VHANEs. The question naturally arises whether nonuniformities in the expansion give rise to new effects. Figure 18 shows the results of three 2-D electromagnetic particle simulations, carried out to late times by expanding the grid, at several points in time. The top expansion is uniform: the y-component of the initial expansion velocity $V_y = V_x$, the initial x-component. (The particles expand radially with velocity $V_r = V_x \cos\theta + V_y \sin\theta$.) The middle panels correspond to $V_y = 0.5V_x$, the bottom panels to $V_y = 0.25V_x$. Except for the anticipated fact that the plasma is more elongated in the asymmetric expansions, there is little difference in the mode structure at early times and the amount of nonlinear coalescence to longer wavelengths is about the same in each case. Of course, the asymmetries (i.e., jets) seen in the laser experiment are a much later manifestation and could likely imply other effects, but at early times, one does not expect the short wavelength physics to be affected very much by asymmetries.

G. 3-D Simulations

We have begun a study of 3-D effects associated with expanding plasmas using a newly developed extension of the explicit electromagnetic particle code ISIS. Here we briefly discuss two aspects of the problem: (1) a comparison of the structuring instability in 2-D and 3-D, and (2) a new effect, streaming of energetic electrons from the cloud along the ambient magnetic field [Barnes, Jones, and Winske, in preparation].

The 2-D simulations are similar to those described in Section 2. The plasma consists initially of a thin cylinder of radius $r_o = 2c/\omega_e$. The electrons and ions both expand radially with velocity $V_r = 0.0136c$, with an electron (and ion) thermal speed of 0.001c, into a magnetic field $B = B_o\hat{z}$ of strength $\Omega_e/\omega_e = 0.8$. 10000 particles on a 50×50 grid were used in the calculation. The left panels of Figure 19 show the ions in the x-y plane at two times, $\omega_{LH}t = 4.8$ and 9.6. As with the simulations described earlier, one sees a thin plasma shell forms and large flute modes grow on the surface.

The 3-D simulation starts with a sphere of identical radius, with the particles expanding with velocity $V_r = 0.02$. The radial velocity has been adjusted so that R_B is the same in both cases [Eq. (7)]. In this case 400000 particles are used on a $50 \times 50 \times 100$ grid. The right panels show the projection of the ions onto the x-y plane at the same two times. While the overall effect of the instability is qualitatively the same, several differences between 2 and 3-D are evident from the figure. First, the size of the flutes in 3-D are larger, suggesting a faster growing instability. Second, the number of flutes in the 3-D case is slightly less. Both of these features are consistent with the larger effective deceleration in 3-D, and the fact that ρ_i/R_B is slightly larger. Third, the 3-D case seems to lack a central cavity; this, however, is a visual effect resulting from projecting all the ions onto one plane. The fact that the flutes are visible in spite of the projection also indicates that

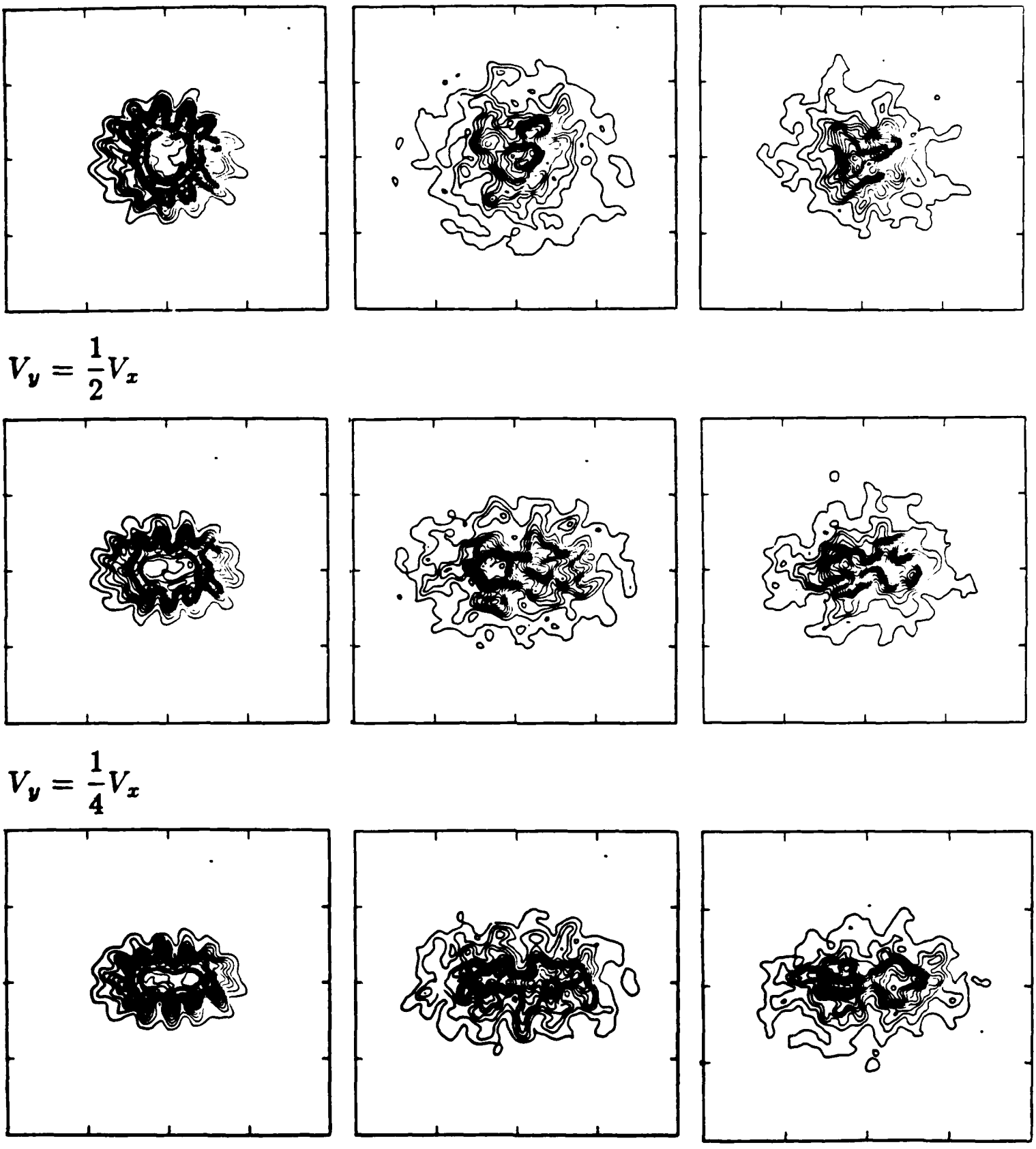

Figure 18. Results of simulations with asymmetric expansion velocities, showing ion density contours at various times: (top panel) $V_x = V_y$; (middle panels) $V_y = V_x/2$; (bottom panels) $V_y = V_x/4$.

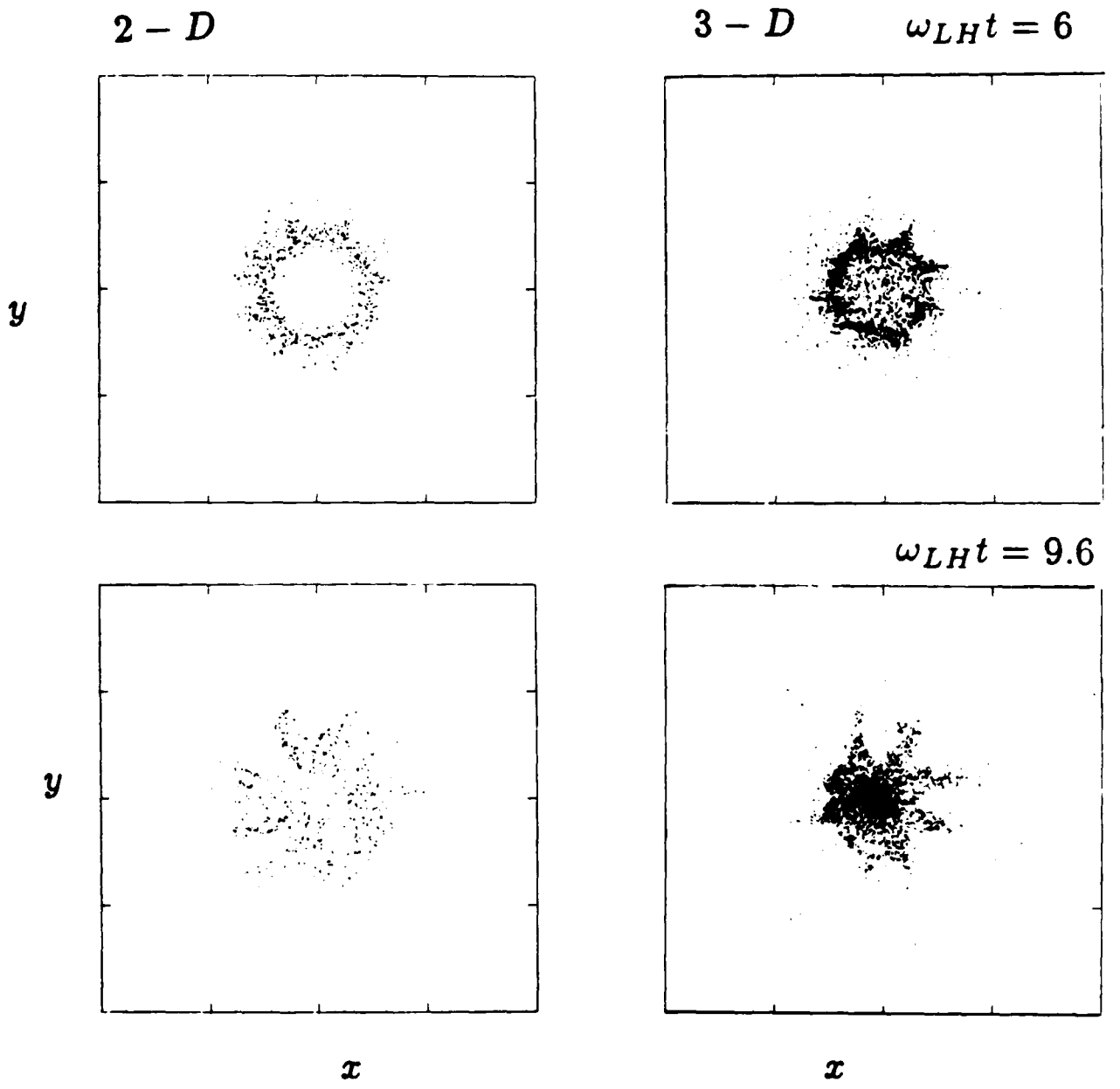

Figure 19. Electromagnetic particle simulations showing ions in x-y plane: (left panels) 2-D run; (right panels) 3-D run.

the structures are field aligned. Finally, there is a marked asymmetry in the 3-D case. Such asymmmetries sometimes also occur in 2-D, and it is not thought to be a peculiarity of 3-D.

However, a new effect is observed in 3-D, as shown in Figure 20. Plotted in the figure are the ions and electrons projected onto the y-z plane at $\omega_{LH}t = 4.8$. Again, several interesting features are visible. First, the shape of the ion cloud and the electron cloud are different. The ion cloud is fatter (in y), which results from the fact that the ions expand slightly ahead of the electrons (recall Figure 1). This is referred to as the "ion charge layer" by Galvez et al. [1988]. Second, the cloud is not spherical. As the expansion stops in the radial direction, the motion of the plasma continues along z. At later times, the cloud becomes even more cigar shaped, as was observed to occur in the AMPTE barium releases [Bernhardt et al., 1987]. Third, and most significant, a small number of electrons have streamed out of the cloud along the magnetic field. This effect is not seen in two-dimensional simulations in which B is in the plane of the calculation.

Two tentative explanations for this phenomenon are as follows. It is observed even in the 2-D simulations where the magnetic field is perpendicular to the plane of the calculations, that in addition to the lower hybrid drift instability that produces the structure on the surface, another instability occurs very early in the run. This instability is only seen when the electrons are very cold, has short wavelength, and serves to heat the electrons to modest temperatures very rapidly. (Note from the discussion of Sec. 3C that the slower growing lower hybrid drift instability is hardly affected by the magnitude of T_e.) It is thought that the instability is some form of the Kelvin-Helmholtz instability, similar to that observed by Sydora et al. [1983] in their electrostatic simulations. The effect of this instability in 3-D is to allow some of the heated electrons to escape as a burst along the magnetic field. And because the instability does not occur in 2-D simulations where B is in the plane of the calculation, the electron streaming is not observed in that case. A second possibility is that the lower hybrid waves heat the electrons. Even though the structures appear to be flute modes ($k_{||} = 0$), it takes only a small component of k along B to accelerate the electrons [e.g., Tanaka and Papadopoulos, 1983]. More study is needed to distinguish between these two mechanisms. Obviously, because the plasma will try to maintain quasineutrality, the amount of electrons which can escape is small. Nevertheless, it can be an important effect and one which we will investigate more completely in the future.

H. Weak Instability Limit

We have seen in Sec. 3D that a strong instability occurs when $\rho_i/R_B \geq 1$. However, the instability can still be excited for $\rho_i/R_B \ll 1$. When $g = 0$, the properties of the lower hybrid drift instability are well known in this weak drift limit. The instability persists down to

$$V_E/v_i = 4(m_e/m_i)^{1/4} \tag{19}$$

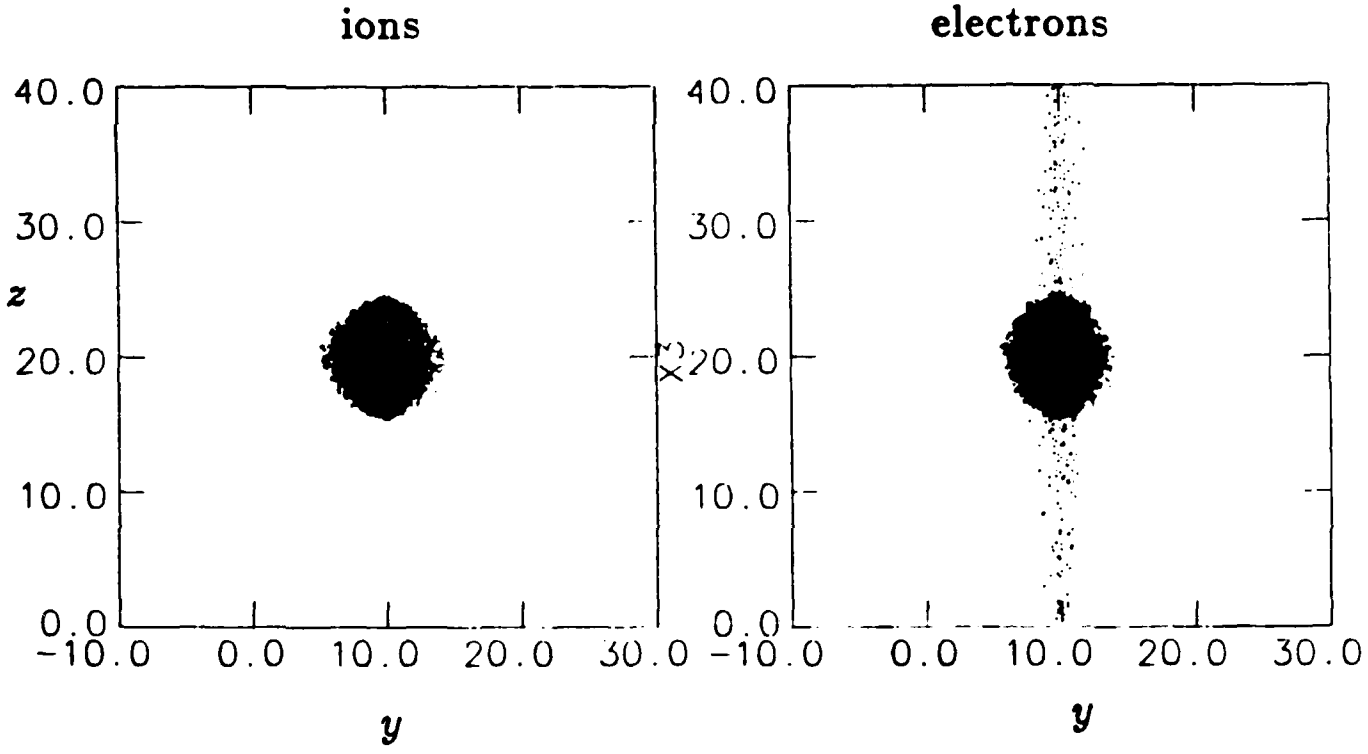

Figure 20. Results of 3-D simulations showing particles projected into y-z plane: ions (left panel), electrons (right panel).

Below this value the unmagnetized ion approximation breaks down ($\omega < \Omega_i$) and ion cyclotron effects stabilize the instability [Freidberg and Gerwin, 1977].

When $g \neq 0$, but $\beta_i \ll 1$, the instability can exist at even very weak drifts. Figure 21 shows the results of linear theory with cold electrons, unmagnetized warm ions with $\epsilon_n c/\omega_i = 2$ and $m_i/m_e = 1836$. Plotted are the growth rates maximized over k as a function of β_i for several values of V_g/v_A. Generally, γ decreases with both V_g/v_A and β_i. But the instability still occurs as $\beta_i \to 0$ for $V_g \neq 0$ and close to $\beta_i = 0$ for $V_g = 0$. (The bottom curve ends where $\omega_r < \Omega_i$, indicating the breakdown of the theory.) Thus, even at $\beta_i = 0.001$, for $V_g/v_A = 0.002$, implying $\rho_i/R_B = 0.0014$ (for a=1.5), one finds $\gamma \simeq 0.08\Omega_i$. And the number of growth times to the end of the expansion is $\gamma t = (\gamma/\Omega_i)(\Omega_i t) \simeq (\gamma/\Omega_i)(1.5R_B/\rho_i) \sim 80$. However, as we show later in this report, even though the growth rate is large and the instability has plenty of time to grow, its effect on diffusion of the magnetic field and heating of the plasma is very weak. While the instability is relatively unimportant in this limit, one must also keep in mind that other long wavelength, $k\rho_i \ll 1$, slower growing modes probably also occur.

I. Collisional Effects

The effect of collisions with the background plasma is important in the laser experiments and affects HANEs at lower altitudes. The study of collisional processes with respect to the usual lower hybrid drift instability has been investigated in some detail for ionospheric applications [Sperling and Goldman, 1980; Huba and Ossakow, 1981; Gary et al., 1983]. Here we carry out a simple analysis when $V_g \neq 0$, in fact $V_g > V_n$, and show that such effects persist and can be important.

The inclusion in the linear theory of collisions with a background plasma and neutrals is straightforward. One replaces ω in the electron terms with $\omega + i\nu_e$ and with $\omega + i\nu_i$ in the ion terms. Here $\nu_e = \nu_{en} + \nu_{ee}k^2\rho_e^2$, where ν_{en} = electron neutral collision frequency and ν_{ee} = the electron-electron collision frequency; similar expressions occur for ν_i [Sperling and Goldman, 1980]. In addition, the presence of ν_i increases the drag of the ions; hence, the magnitude of the radial electric field and thus V_E:

$$eE_r = m_i\frac{dV_i}{dt} - T_i\epsilon_n - m_i\nu_i V_i \tag{20}$$

which implies an increased deceleration $g = -dV_i/dt + \nu_i V_i$. Figure 22 displays growth rates versus k for the same parameters as Figure 3, on the same scale for easy comparison. Here we have assumed $T_e = 0$ and included only the electron-neutral and ion-neutral collisions. The addition of $\nu_e \neq 0$ reduces the maximum growth rate but does not shift the wavelength corresponding to the most unstable mode (as would occur with $T_e \neq 0$). Even with $\nu_e = 100\Omega_i \sim 2\gamma$ the maximum linear growth rate is not reduced very much. However, the addition of ion collisions (here $\nu_i = 20\Omega_i$) has a marked effect on the growth of the instability [Gary et al., 1983].

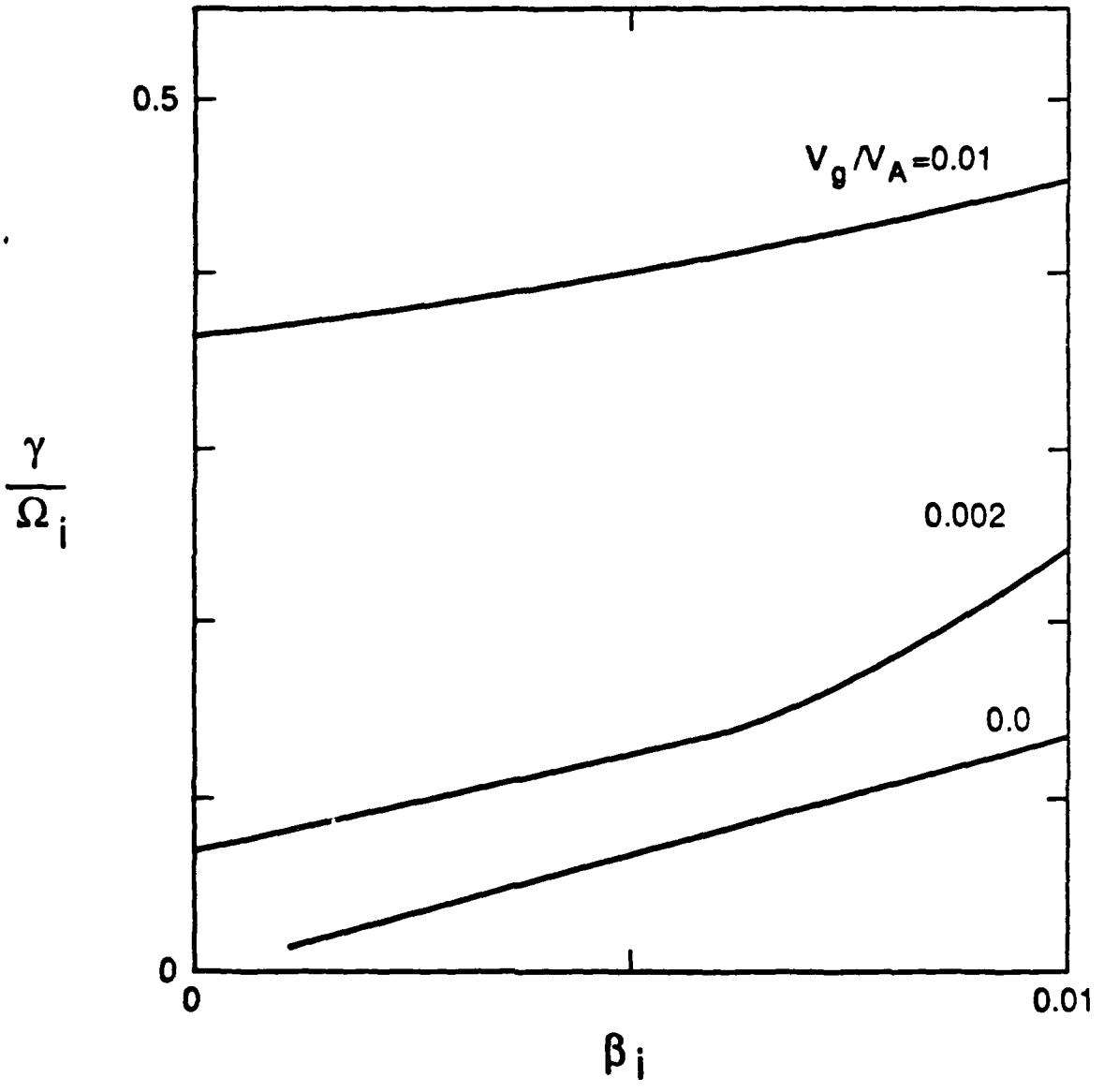

Figure 21. Results of linear theory with cold electrons showing growth rates maximized over wavenumber versus β_i for various values of V_g/v_A. The bottom curve cuts off when $\omega_r < \Omega_i$, indicating the breakdown of the assumption of unmagnetized ions.

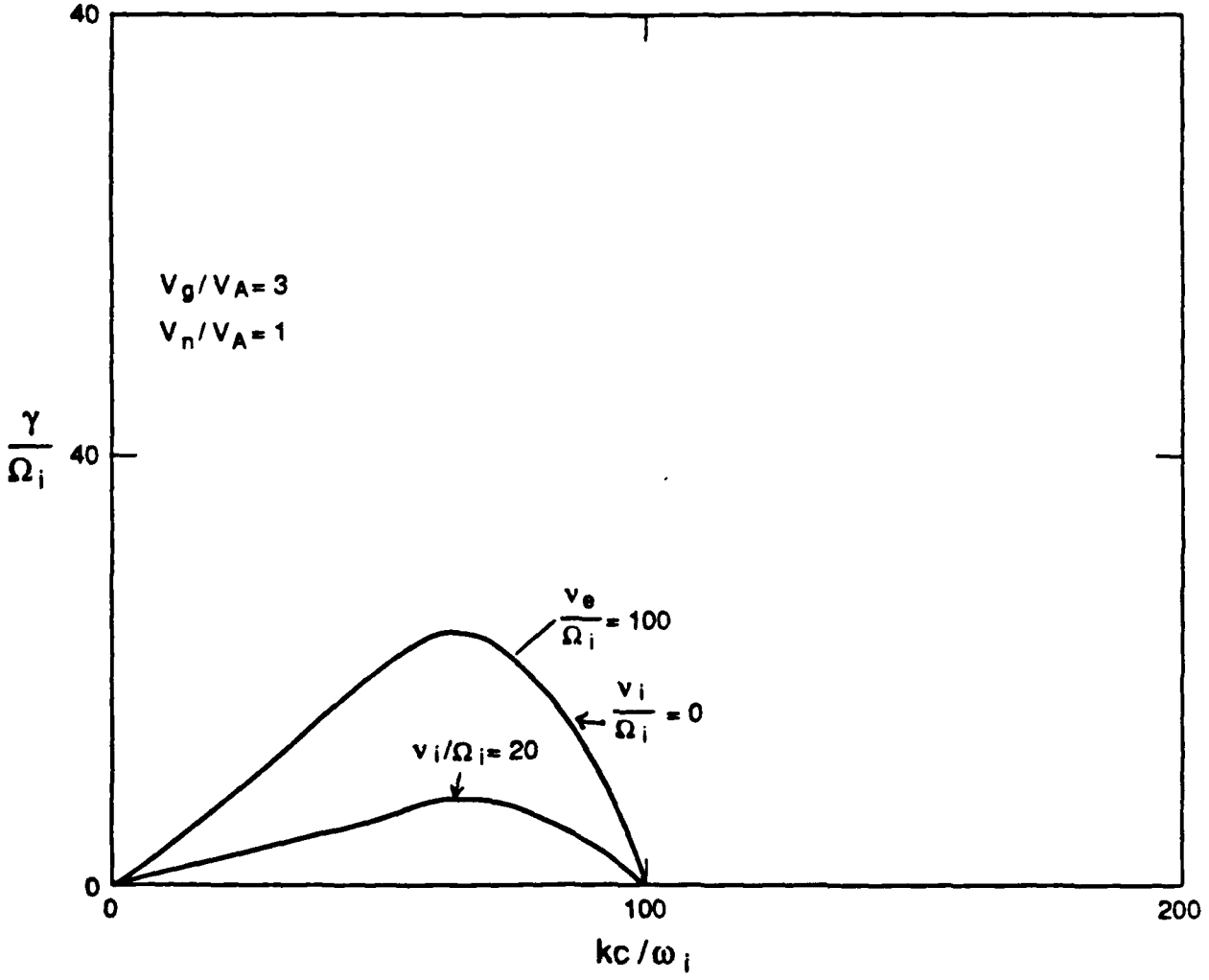

Figure 22. Results of linear theory showing growth rates as a function of wavenumber for same parameters as Figure 3, except that $\nu_e = 100\Omega_i$ and $\nu_i = 0$ (top curve), $\nu_i = 20\Omega_i$ (bottom curve).

The fact that the instability persists for very large values of ν_e is well known [Gary et al., 1983]. Figure 23 shows growth rates maximized over wavenumber versus ν_e/Ω_i for various values of V_g/v_A (with $V_n/v_A = 1$, $\beta_i = 0.2$, $T_e = 0$, $\nu_i = 0$). With $V_g = 0$ (the usual lower hybrid drift instability) the inclusion of collisions strongly reduces the maximum growth rate, but does not change the wavenumber corresponding to maximum growth very much. An extension of the initial fall off of the curve with ν_e would imply stability when $\nu_e \sim \gamma(\nu_e = 0)$. However, another branch of the instability (the collisional density drift instability of Gary et al. [1983]) takes over and gives significant growth for $\nu_e \gg \Omega_i$. At $V_g \neq 0$, these two distinct modes merge into one, with γ falling off slowly with ν_e.

The effect of collisions on the instability has been tested by simulations using VENUS, a 2-D electromagnetic particle code which allows collisional interactions [Cranfill et al., 1986]. In this preliminary study Rutherford scattering between the expanding plasma particles, rather than Krook collisions with a background gas that was assumed in the linear theory was used. Nevertheless, the effect that the instability may persist for relatively high rates of collisions (relative to the linear growth rate) appears to occur. Figure 24 shows snapshots of four runs at one instant of time. For each run the ions in x-y space, contours of ion density, and magnetic field contours are shown. From top to bottom the collision frequency was varied from $\nu_e = 0, 0.1, 10, 100\omega_{LH}$ ($\nu_e/\nu_i \simeq 30$). For large collision frequencies the plasma does not expand very much, as the directed motion is quickly thermalized with only a few energetic particles escaping. Nevertheless, an instability at roughly constant wavelength appears in each case. Obviously, much more work using a collision model consistent with the theory needs to be carried out, but the initial results are encouraging.

4. Discussion

This final section consists of three parts: (A) a discussion of issues regarding the theoretical work and its relation to the laser experiments, (B) the consequences of the results for very high altitude nuclear explosions, and (C) a short summary.

A. Laser Experiments

The results presented in this report raise a number of questions regarding the findings of the several laser experiments in which structures on expanding plasmas have been observed. We subdivide the subsequent discussion into four areas: (1) properties of the observed waves, (2) ρ_i/R_B effects, (3) late time behavior, and (4) collisional effects.

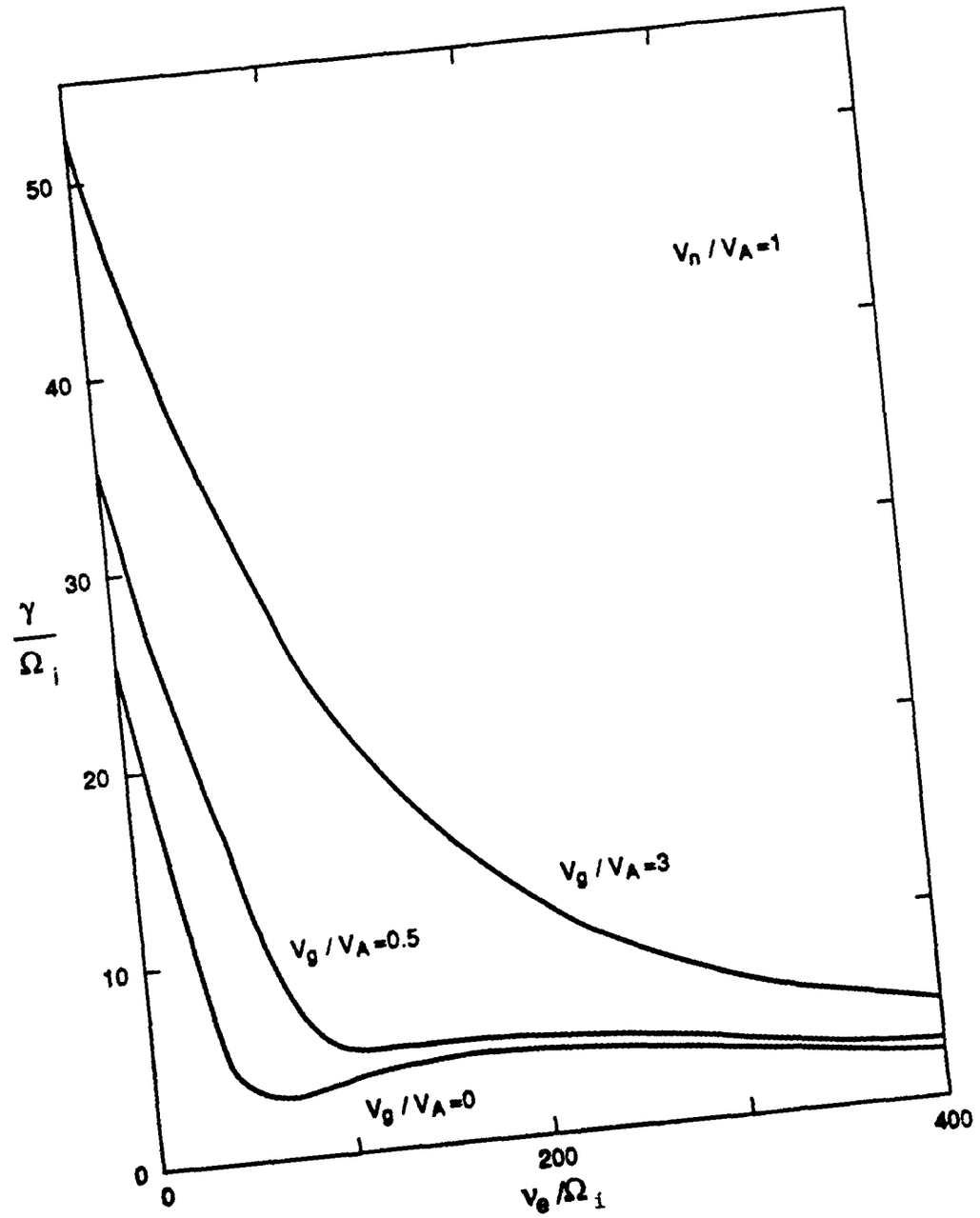

Figure 23. Linear growth rates maximized over k versus ν_e for various values of V_g/v_A with $\nu_i = 0$.

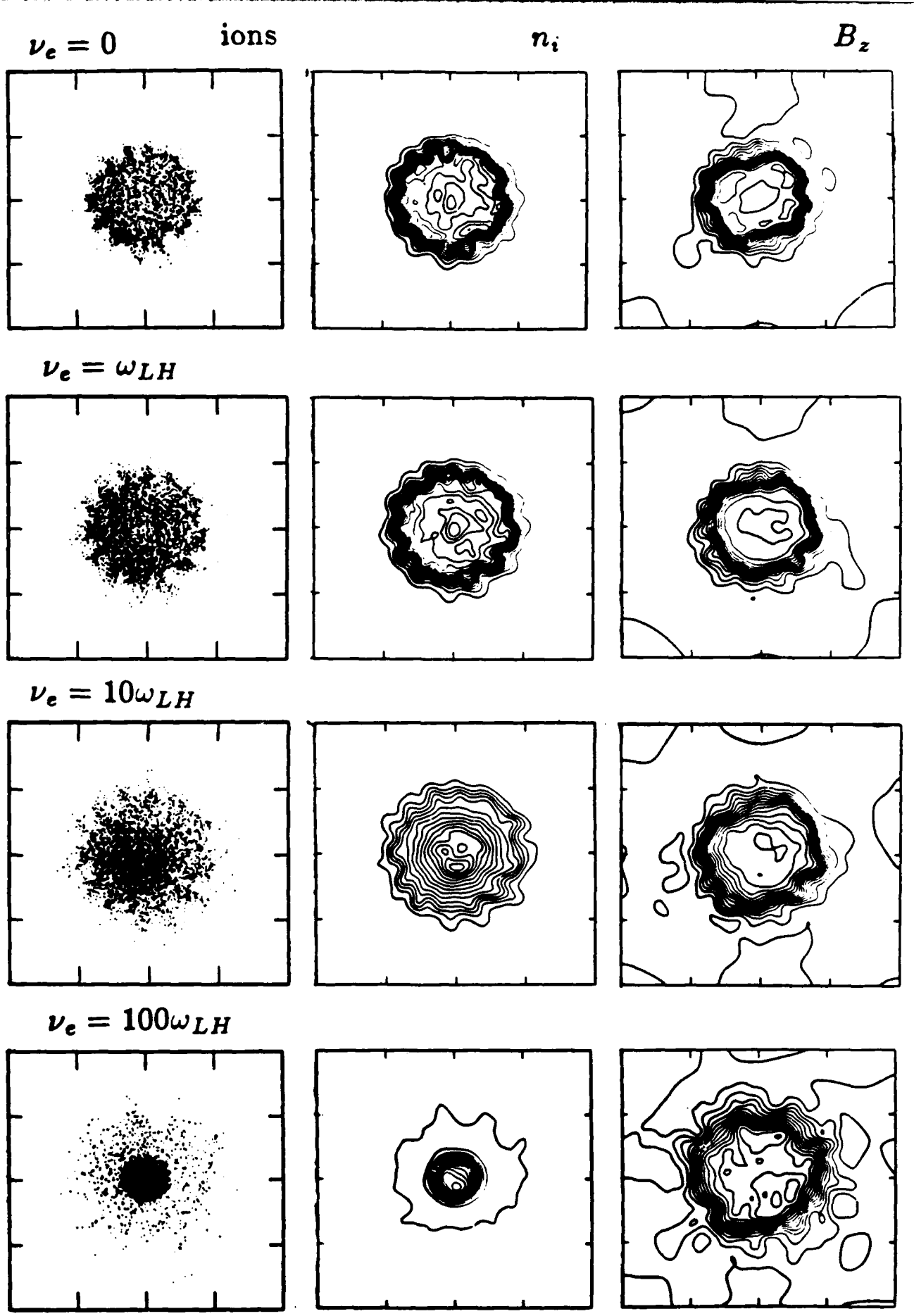

Figure 24. Results of 2-D electromagnetic particle simulations with Rutherford collisions: ions in real space, ion density contours, and magnetic field contours at one time for four runs with different values of the collision frequency.

1. Observed Waves

The key question is what is the relation of the waves observed in the simulations to those seen in the experiments. It has been argued that the lower hybrid drift instability cannot be responsible for the structures seen on the surface because the theoretical wavelengths are much too small compared to those measured in the NRL experiments [Ripin et al., 1987] and in the AMPTE magnetotail releases [Bernhardt et al., 1987]. Such estimates are usually based on the expression $k\rho_e \simeq 1$ ($T_e \simeq T_i$) and assuming a very cold electron temperature. However, we have seen that important linear modifications including $g \neq 0$ (Sec. 2), correct inclusion of 3-D dynamics (Sec. 3A), finite β_e (Sec. 3B) and nonlinear effects (Sec. 3D) all operate to push the theoretical value of k to smaller values. There are also other effects, e.g., nonlocal theory with electromagnetic corrections and realistic radial profiles, which would also modify the wavelength of the instability. A related difficulty with comparing with experiments is that often the parameters, such as the local value of the deceleration and the ion temperature, are not known with much certainty. In addition, other effects, such as the changing charge state of the aluminum plasma in the NRL experiment, that are not included in the theory as yet, may also be important.

A second issue involving the wavelength of the surface flutes is how they scale with the applied magnetic field, B_o. While the Japanese experiments show $k \sim B_o^{0.8}$, the NRL experiments do not show any consistent variation of k with B_o. One possible explanation is suggested by the simulations and was shown in Figure 5. Measurements of k during the linear growth phase indicated $k \sim B_o^{0.5}$, consistent with linear theory when k was normalized to R_B. However, during the nonlinear phase when the modes coalesced, k was roughly independent of B_o. It may be that in the NRL experiments (at larger ρ_i/R_B) that one is observing the structures in their nonlinear state, rather then while they are growing exponentially according to linear theory, which may be more characteristic of the Okada et al. [1981] observations. This question may be resolved when the NRL experiment acquires the capability to make multiple observations per shot. In a similar vein, it would be useful to examine the variation of the wavelengths of the flutes with the ion to electron mass ratio, by changing the laser target material. Figure 5 suggests a weak $(m_i/m_e)^{1/4}$ dependence in both the linear and nonlinear regimes, as do the simulations of Sgro et al. [1988].

A related issue involves the real frequency of the waves. Both the laser experiments and the simulations show flutes that appear to be stationary, implying $\omega_r \simeq 0$. However, the most unstable modes according to linear theory are characterized by $\gamma \sim \omega_r \sim \omega_{LH}$. The simulations do show, however, that by the time the flutes are visible in the particles (which would correspond to optical observations) that the waves are already rather nonlinear ($e\delta\phi/T_i > 1$). At early times the frequency is large ($\omega_r \sim \omega_{LH}$), but the phase velocities are small because k is large. At later time the nonlinearities produce phase shifts of the frequency so that $\omega_r \rightarrow 0$. Indeed such phase shifts would allow the mode coupling process to proceed more easily by allowing the k's and ω's to satisfy the matching conditions, $k_o = k_1 + k_2$, $\omega_o = \omega_1 + \omega_2$. Such nonlinear frequency shifts are well known to occur for the lower hybrid drift instability with $g = 0$ [Winske and Liewer, 1978].

All the laser experiments [Ripin et al., 1987; Okada et al., 1981; Zakharov et al., 1986] also detected high frequency plasma noise in the lower hybrid frequency range. Similar noise was measured by the AMPTE/IRM satellite [Gurnett et al., 1986] at the edge of the cavity in both the electric and magnetic receivers. Because the lower hybrid drift instability is essentially an electrostatic mode, but also has an electromagnetic component, it is the likely source of the noise. However, since the instability is not sharply peaked in frequency, one expects a broad, rather featureless spectrum is generated, consistent with the measurements. Even though we have previously argued that the dominant modes may nonlinearly shift their frequency to smaller values, a range of low amplitude waves will still be continuously generated and provide a broad frequency spectrum. Although the spectrum is broad, the fact that the frequency centers on ω_{LH} suggests looking for shifts in the bandwidth with the applied magnetic field and the mass of the ions.

A final issue concerns the characteristics of the observed structures in asymmetric expansions. Our simulations, which describe the early time behavior, suggest that asymmetries in the expansion do not affect the properties of the short wavelength modes nor their coalescence to larger structures appreciably. The principal effect would come from a modified effective deceleration (g) which an asymmetry could produce. A study of the wavelengths of the observed flutes as the asymmetry is varied (by changing the angular spread of the laser) could shed future light on this question.

2. ρ_i/R_B Effects

Various experiments have shown, and the simulations here have confirmed, that the single most important parameter is ρ_i/R_B. When $\rho_i/R_B > 1$, as in the NRL experiments, large flutes are observed that display interesting nonlinear dynamics and the size of the magnetic cavity (R_M) is less than R_B [Zakharov et al., 1986]. When $\rho_i/R_B \leq 1$, as in the AMPTE releases, the Japanese laser experiments, and theta pinches, the flutes are smaller and exhibit less dramatic behavior, while $R_M \simeq R_B$. When $\rho_i/R_B \ll 1$, as in the hot diamagnetic cavities upstream of the Earth's bow shock (and probably also a VHANE), only a very weak instability is detected. Such results are also consistent with theory in that $\rho_i/R_B \sim V_g/v_A$. For moderately cold plasmas the contribution to the cross-field drift due to V_g is greater than that due to the usual diamagnetic drift V_n, so that V_g is a direct measure of the free energy of the instability.

A most useful set of laser experiments would be to vary ρ_i/R_B systematically. In 2-D, as in the simulations, both R_B and ρ_i vary as B_o^{-1}, so ρ_i/R_B is independent of B_o; however, in 3-D $R_B \sim B_o^{-2/3}$, so $\rho_i/R_B \sim B_o^{-1/3}$. Other ways to change ρ_i/R_B would be to either decrease the laser energy so that the streaming velocity V_D is reduced, $\rho_i/R_B \sim V_D^{-1/3}$, or change the target material to alter the ion mass. One would like to quantify the wavelengths and the radial extent of the flutes (relative to R_B). A more difficult measurement would be the size of the magnetic cavity compared to R_B, again for a range of ρ_i/R_B [e.g., Zakharov et al., 1986].

3. Nonlinear Effects

The surface modes generated in the $\rho_i/L_B > 1$ regime exhibit a number of interesting, probably nonlinear effects. These include the freestreaming of the flute tips, bending of the flutes in the magnetic field, and bifurcation of the ends of the structures [Ripin et al., 1987].

The simulations carried out in this regime show a number of similar features [Winske, 1987]. Continued outward streaming of the flutes is seen, while the inner portion of the plasma and the magnetic cavity recollapse [e.g., Figures 4 and 12]. Bending of the flutes is often observed, although the sense of the bending is usually opposite to the experiments. The flutes in the simulations bend clockwise, following the ion sense of rotation, rather the electron sense. An exception are the hybrid simulations of Sgro et al. [1988], where the flutes bend in the electron sense. In this case, however, the current seems to be carried mainly by the ions, which have a large diamagnetic drift.

Furthermore, the simulations clearly show mode coalescence and later the reappearance of shorter wavelength modes [e.g., Figure 14]. It appears from an analysis of the simulations that these short wavelength structures are remnants of the original linear modes, rather than bifurcation of the larger structures. It would be interesting in both the simulations and the laser experiments to check if these larger k modes exhibit some dependence on B_o, as do the waves in the linear regime.

4. Collisional Effects

A final effect that we have studied involves collisions with the background plasma. Both linear theory and the particle simulations suggest that the instability can persist for very large values of the electron-neutral collision frequency at roughly the same wavelength. On the other hand, ion collisions serve to both increase the effective deceleration (which increases the growth rate slightly) and more importantly, to damp the waves.

In the laser experiments the collision frequency can be varied by changing the fill pressure of the background gas. The experiments at NRL suggest that as the fill pressure is raised, the instability is less easy to see optically, retains about the same wavelength, and is eventually quenched if the background pressure is too high. Overall, these qualitative results are consistent with the simple theoretical analysis that has been done so far. A more careful study of this effect experimentally both as a function of fill pressure and if possible T_e/T_i, to change ν_e/ν_i, would be useful.

B. Consequences for VHANE

We next turn to a very different parameter regime, that of a very high altitude nuclear explosion (> 1000 km). Assuming a weapon yield of about one megaton with about a quarter of the energy going into kinetic energy of the debris ions, yields about $N \sim 10^{28}$

ions. Assuming an expansion velocity of 2×10^3km/sec and a simple pressure balance relationship (7) with $B_o = 1/3G$ gives $R_B \simeq 800$km. Taking $A = 27$, $Z = 13$ for an "average" ion, one finds $\rho_i \sim 1.3$ km. Thus, $\rho_i/R_B = 1.6 \times 10^{-3}$ and $V_g/v_A = 1.5\rho_i/R_B = 2.4 \times 10^{-3}$, in contrast to the laser experiments and simulations where $\rho_i/R_B \sim 1$ Furthermore, taking the plasma temperature ~ 10 keV yields $\beta_i = 0.002$ at maximum expansion, which for $\epsilon_n c/\omega_i \sim 2$ gives $V_n/v_A = 0.002$. Thus, although one has $V_g/v_A \ll 1$ and $V_n/v_A \ll 1$, still $V_n \sim V_g$, as in the simulations.

Even though the gradients and cross-field drifts are very small under these conditions, the lower hybrid drift instability is still excited. Figure 18 shows growth rates maximized over wavenumber versus β_i in this regime. Under conditions expected for a VHANE, the growth rate is still significant $\gamma/\Omega_i \sim 0.1$. As shown in Sec. 3H, the number of e-foldings in this regime is large, so that $\gamma t \sim 100$. But the important question remains, how large are the anomalous effects associated with the instability in this case.

Figure 18 shows that for β_i small, $\gamma \sim \beta_i \sim (V_E/v_i)^2$. This weak drift limit for the usual (no g) lower hybrid drift instability has been investigated in much detail. Both the linear properties of the waves [Davidson and Gladd, 1975] and their nonlinear consequences [Brackbill et al., 1984] are well understood. Here we will use some of these known properties to estimate what will happen in a VHANE. Unfortunately, the $\rho_i/R_B \ll 1$ regime is not readily accessible to simulations, as the instability is so weak.

The anomalous collision frequency for the lower hybrid drift instability is given by Liewer and Davidson [1977]:

$$\nu_{an} \simeq (\frac{\pi}{2})^{1/2} \frac{\omega_e^2}{\Omega_e^2} \omega_{LH} (\frac{V_E}{v_i})^2 \frac{\epsilon_F}{n m_e V_E^2/2} \tag{21}$$

For a VHANE, we take $V_E = V_g + V_n \sim 2V_n$; $(V_E/v_i)^2 \sim 4(V_n/v_i)^2 \sim 4\beta_i$ and take ϵ_F =the nonlinear fluctuation level of the waves $\simeq n m_e V_E^2/2$ [Brackbill et al., 1984]. At $r = R_B$ the debris density is $n \sim 5 \times 10^3$ so that $\omega_e^2/\Omega_e^2 \sim 1$ and $\nu_{an} \sim 0.0045\omega_{LH} \simeq \Omega_i$. Using this value and following the discussion of Sec. 3D we can calculate the amount of anomalous diffusion expected: $\Delta x^2 \sim Dt \sim \varsigma V_D^2 \Omega_i^2 (\rho_i/R_B)^3 t^4$ or $\Delta x/R_B \sim 10^{-4}$, which is negligible. In other words, the plasma expansion is essentially classical with regard to this instability. (Of course, other types of slower growing, longer wavelength instabilities that we have not considered here can still be operative.)

In similar fashion one can calculate the anomalous heating rate for the ions, $Q_{an}^i \sim \nu_{an}$ [Liewer and Davidson, 1978]

$$\frac{1}{T_i} \frac{dT_i}{dt} \sim Q_{an}^i \frac{m_e V_E^2}{3T_i} \simeq 2 \times 10^{-9}\, \Omega_i \tag{22}$$

So negligible ion (as well as electron) heating is likely. In addition, it was noted in Sec. 3G that electron acceleration and streaming along the magnetic field may occur during the

expansion. However, such effects require very cold electrons initially and perhaps special initial conditions, as well as significant deceleration. None of these conditions is likely to occur early in a VHANE. Thermal (i.e., $\sim$ 10 keV) electrons will have a directed velocity comparable to their thermal speed and for $\rho_i/R_B \ll 1$ the deceleration will be weak. Acceleration of electrons by lower hybrid waves [e.g., Tanaka and Papadopoulos, 1983] is also possible, and seen in the 3-D simulations, but again is not likely due to the very low level of fluctuations.

Thus, one does not expect the lower hybrid drift instability to be very important for VHANES. It is most likely that the cavity expands in almost a classical fashion to its maximum radius, with a low level of short wavelength fluctuations on the surface. Because the instability is expected to be so weak, no strong nonlinear effects are likely to occur: i.e., no large scale flutes are expected to form and break off. And because the diffusion is very small, the plasma will contract radially and continue to expand axially. Of course, the large size of the cavity and how it interacts with the Earth's diverging magnetic field has yet to be included in the analysis. But such processes can be considered in the absence of strong anomalous processes fairly easily.

That such large scale cavities are rather benign is not suprising. Large diamagnetic cavities occur upstream of the Earth's bow shock. These typically are larger than one Earth radius ($R_E \sim$ 6400km), while ρ_i for a typical solar wind proton ($V_D \sim$ 500km, $B = 10^{-4}$G) is about 500 km so that $\rho_i/R_B < 0.1$. Although one is limited by the usual problem of separating temporal and spatial behavior with single spacecraft measurements, there is no indication that large scale surface structures or asymmetries exist [Thomsen et al., 1986]. Although plasma noise is detected at the surface of the cavity, the measured gradients and plasma temperature do not suggest strong anomalous effects. The ground based and spacecraft observations of the cavity produced by the AMPTE barium releases in the magnetotail in which $\rho_i/R_B \sim 1$ again were consistent with a rather nonviolent behavior. [Bernhardt et al., 1987]. The observed flutes were small, did not seem to grow into extended fingers, and the collapse of the cavity according to classical behavior again suggested a very nondramatic instability

One area where the instability may be relevant, however, is to lower altitude bursts, like CHECKMATE, at very early times. In such situations collisional effects with the background can be important. We have seen that the lower hybrid drift instability can persist in the presence of large collision frequencies in Sec. 3I. A separate report in preparation discusses possible application of the lower hybrid drift instability in this more collisional regime.

C. Summary

To sum up briefly, in this report we have discussed a number of issues related to early time structuring in very high altitude nuclear explosions and in laser experiments that study some of the physics. Our emphasis has been on retaining electron effects in the

analysis throughout. The inclusion of electron physics determines a scale length on which the fastest growing structures develop. We have shown how the longer wavelength effects that are observed can arise from these smaller seed structures. We have reviewed the basic mechanism of the instability, the results of a linear analysis based on cold electrons, and particle simulations in which both electron and ion kinetics are included. Furthermore, we have discussed a number of enhancements to the model, both in the linear theory and in the interpretation of a number of simulations carried out over a range of parameters. We have also related the results to the interpretation of the NRL observations and suggested some experimental tests of the theory. Finally, we have addressed how the theory scales to the VHANE situation and indicated areas for further study in this regime.

Acknowledgements

We acknowledge useful and stimulating discussions with Drs. K. Akimoto, S. H. Brecht, S. P. Gary, K. Quest, B. H. Ripin, and V. A. Thomas. Contributions from Drs. C. Barnes, M. Gaivez, D. S. Lemons, M. E. Jones, and A. G. Sgro are gratefully appreciated. This work was performed under the auspices of the U. S. Department of Energy, and was supported by the Defense Nuclear Agency under Project Code RB, Task Code RC, Work Unit Code 167, and Work Unit Title "Simulations and Modeling of HANE/VHANE."

References

Akimoto, K., M. Galvez, S. P. Gary, A. G. Sgro, and D. Winske, Prompt structuring of a plasma expanding in an external magnetic field, *J. Geomag. Geoelect.*, in press, 1988.

Batchelor, D. B., and R. C. Davidson, Nonlocal analysis of the lower hybrid drift instability in theta-pinch plasmas, *Phys. Fluids, 19*, 882, 1976.

Bernhardt, P. A., R. A. Roussel-Dupre, M. B. Pongratz, G. Haerendel, A. Valenzuela, D. A. Gurnett, and R. R. Anderson, Observations and theory of the AMPTE magnetotail barium releases, *J. Geophys. Res., 92*, 5777, 1987.

Brackbill, J. U., D. W. Forslund, K. B. Quest, and D. Winske, Nonlinear evolution of the lower hybrid drift instability, *Phys. Fluids, 27*, 2684, 1984.

Brecht, S. H., and K. Papadopoulos, Cross field jetting of energetic ions produced by Rayleigh-Taylor instability, NRL Memo Report 4068, 1979.

Brecht, S. H., and V. A. Thomas, Multidimensional simulations using hybrid particle codes, *Comput. Phys. Comm., 48*, 135, 1988.

Cranfill, C. W., J. U. Brackbill, and S. R. Goldman, A time implicit Monte Carlo collision algorithm for particle in cell electron transport models, *J. Comput. Phys., 66*, 23 1986.

Davidson, R. C., and N. T. Gladd, Anomalous transport associated with the lower hybrid drift instability, *Phys. Fluids, 18*, 1327, 1975.

Davidson, R. C., N. T. Gladd, C. S. Wu, and J. D. Huba, Effects of finite plasma beta on the lower hybrid drift instability, *Phys. Fluids, 20*, 301, 1977.

Drake, J. F., P. N. Guzdar, A. B. Hassam, and J. D. Huba, Nonlinear mode coupling theory of the lower hybrid drift instability, *Phys. Fluids, 27*, 1148, 1984.

Drake, J. F., J. D. Huba, and N. T. Gladd, "Stabilization" of the lower hybrid drift instability in finite beta plasmas, *Phys. Fluids, 26*, 2247, 1983.

Fahrbach, H. U., W. Koppendorfer, M. Munich, J. Neuhauser, H. Rohr, G. Schramm, J. Sommer, and E. Holzhauer, Measurement of lower hybrid drift fluctuations in the boundary layer of a high beta plasma by collective CO_2 laser light scattering, *Nucl. Fusion, 21*, 257, 1981.

Freidberg, J. P., and R. A. Gerwin, Lower hybrid drift instability at low drift velocities, *Phys. Fluids, 20*, 1311, 1977.

Galvez, M., S. P. Gary, C. Barnes, and D. Winske, Computer simulations of plasma expansion across a magnetic field, *Phys. Fluids, 31*, 1554, 1988.

Gary, S. P., P. A. Bernhardt, and T. E. Cole, Density drift instabilities and weak collisions, *J. Geophys. Res.*, *88*, 2103, 1983.

Gisler, G., Axisymmetric particle-in-cell simulations of diamagnetic cavity formation in a vacuum, *IEEE Trans. Plasma Sci.*, submitted, 1988.

Gisler, G., and D. S. Lemons, Dynamics of a plasma expanding into a uniform magnetic field, *J. Geophys. Res.*, submitted, 1988.

Gurnett, D. A., R. R. Anderson, P. A. Bernhardt, H. Luhr, G. Haerendel, O. H. Bauer, H. C. Koons, and R. H. Holzworth, Plasma waves associated with the first AMPTE magnetotail barium release, *Geophys. Res. Lett.*, *13*, 644, 1986.

Hassam, A. B., and J. D. Huba, Structuring in the AMPTE magnetotail barium releases, *Geophys. Res. Lett.*, *14*, 60, 1987.

Hassam, A. B., and J. D. Huba, Magnetohydrodynamic equations for systems with large Larmor radius, *Phys. Fluids*, *31*, 318, 1988.

Huba, J. D., and S. L. Ossakow, On 11 cm irregularities during equatorial spread F, *J. Geophys. Res.*, *86*, 829, 1981.

Huba, J. D., J. G. Lyon, and A. B Hassam, Theory and simulation of the Rayleigh Taylor instability in the large Larmor radius limit, *Phys. Rev. Lett.*, *59*, 2971, 1987.

Keilhacker, M., M. Kornherr, H. Niedermeyer, F. Soldner, and K. -H. Steuer, Flute instabilities during fast magnetic compression of collisionless $\beta = 1$ plasmas, *Phys. Rev. Lett.*, *32*, 1044, 1974.

Krimigis, S. M., G. Haerendel, R. W. McEntire, G. Paschmann, and D. A. Bryant, The active magnetospheric particle tracers explorers (AMPTE) program, *Eos (Trans)*, *63*, 843, 1982.

Liewer, P. C., and R. C. Davidson, Sheath broadening by the lower hybrid drift instability in post implosion theta pinches, *Nucl. Fusion*, *17*, 85, 1977.

Mendis, D. A, and H. L. F. Houpis, The cometary atmosphere and its interaction with the solar wind, *Rev. Geophys. Space Phys.*, *20*, 885, 1982.

Neubauer, F. M., Giotto magnetic field results on the boundaries of the pile-up region and the magnetic cavity, *Astron. Astrophys.*, *187*, 73, 1987.

Okada, S., K. Sato, and T. Sekiguchi, Possibility of lower hybrid drift instability in laser produced plasma in a uniform magnetic field, *J. Phys. Soc. Japan.*, *46*, 355, 1979.

Okada, S., K. Sato, and T. Sekiguchi, Behavior of laser produced plasma in a uniform magnetic field–plasma instabilities, *Japan J. Appl. Phys.*, *20*, 157, 1981.

Papadopoulos, K., A. Mankofsky, and A. Drobot, Long range cross-field ion beam propagation in the diamagnetic regime, *Phys. Rev. Lett., 61*, 94, 1988.

Peter, W., A. Ron, and N. Rostoker, Instability of the boundary layer between a streaming plasma and a vacuum magnetic field, *Phys. Fluids, 26*, 2276, 1983.

Ripin, B. H., E. A. McLean, C. K. Manka, C. Pawley, J. A. Stamper, T. A. Peyser, A. N. Mostovych, J. Grun, A. B. Hassam, and J. D. Huba, Large Larmor radius interchange instability, *Phys. Rev. Lett., 59*, 2299, 1987.

Sgro, A. G., S. P. Gary, and D. S. Lemons, Expanding plasma structure and its evolution toward long wavelengths, *Phys. Fluids*, submitted, 1988.

Sperling, J. L., and S. R. Goldman, Electron collisional effects on lower hybrid drift instabilities in the ionosphere, *J. Geophys. Res., 85*, 3494, 1980.

Sydora, R. D., J. S. Wagner, L. C. Lee, and E. M. Wescott, Electrostatic Kevin-Helmholtz instability in a radially injected plasma cloud, *Phys. Fluids, 26*, 2986, 1983.

Tanaka, M., and K. Papadopoulos, Creation of high energy electron tails by means of the modified two stream instability, *Phys. Fluids, 26*, 1697, 1983.

Thomas, V. A., and S. H. Brecht, Two-dimensional simulation of high Mach number plasma interactions, *Phys. Fluids, 29*, 2444, 1986.

Thomsen, M. F., J. T. Gosling, S. A. Fuselier, S. J. Bame, and C. T. Russell, Hot diamagnetic cavities upstream from the Earth's bow shock, *J. Geophys. Res., 91*, 2961, 1986.

Thomsen, M. F., J. T. Gosling, S. J. Bame, K. B. Quest, C. T. Russell, and S. A. Fuselier, On the origin of hot diamagnetic cavities near the Earth's bow shock, *J. Geophys. Res., 93*, in press, 1988.

Wessel, F. J., A. Fisher, N. Rostoker, and J. Song, Neutralized ion beam propagation in a transverse magnetic field in vacuum and in plasma, *Phys. Fluids*, submitted, 1988.

Winske, D., Application of particle simulations to the NRL laser experiment, Los Alamos Unclassified Report, LAUR-87-4072, 1987.

Winske, D., Short wavelength modes on expanding plasma clouds, *J. Geophys. Res. 93*, 2539, 1988.

Winske, D., and P. C. Liewer, Particle simulation studies of the lower hybrid drift instability, *Phys. Fluids, 21*, 1017, 1978.

Zakharov, Yu. P., A. M. Orishich, A. G. Ponomarenko, and V. G. Posukh, Effectiveness of the slowing of expanding clouds of diamagnetic plasma by a magnetic field (experimental), *Sov. J. Plasma Phys.*, *12*, 674, 1986.

Zhou, Y. M., H. K. Wong, C. S. Wu, and D. Winske, Lower hybrid drift instability with temperature gradient in a perpendicular shock wave, *J. Geophys. Res.*, *88*, 3026, 1983.

DISTRIBUTION

Dr. B. H. Ripin
Code 4732
Naval Res. Lab.
Washington, DC 20375

Dr. E. McLean
Code 4732
Naval Res. Lab.
Washington, DC 20375

Dr. J. Stamper
Code 4732
Naval Res. Lab.
Washington, DC 20375

Dr. Paul Bernhardt
Code 4780
Naval Res. Lab.
Washington, DC 20375

Dr. Walter Chesnut
SRI International
333 Ravenswood Ave.
Menlo Park, CA 94025

Dr. J. L. Sperling
JAYCOR
11011 Torreyana Road
P. O. Box 85154
San Diego, CA 92138

Dr. R. Stellingwerf
Mission Research Corp.
1720 Randolph Rd. S. E.
Albuquerque, NM 87106

Dr. R. Peterkin
Mission Research Corp.
1720 Randolph Rd. S. E.
Albuquerque, NM 87106

Dr. K. Hain
Maxwell S-Cubed Div.
1800 Diagonal Rd.
Alexandria, VA 22314

Dr. E. Hyman
SAIC
1710 Goodridge Dr.
McLean, VA 22102

Dr. J. Guillory
PRC
5850 Leesburg Pike # 23
Falls Church, VA 22041

Dr. L. Wittwer
RAAE
Defense Nuclear Agency
Washington, DC 20305

Dr. B. Prasad
RAAE
Defense Nuclear Agency
Washington, DC 20305

Director (2)
Attn: STTI
Defense Nuclear Agency
Washington, DC 20305-1000

Dr. R. W. Kilb
Mission Research Corp.
P. O. Box 719
Santa Barbara, CA 93102

Dr. W. W. White
Mission Research Corp.
P. O. Box 719
Santa Barbara, CA 93102

Dr. M. Hausman
Mission Research Corp.
P. O. Box 719
Santa Barbara, CA 93102

Dr. D. Sowle
Mission Research Corp.
P. O. Box 719
Santa Barbara, CA 93102

Prof. D. Papadopoulos
Astronomy Program
University of Maryland
College Park, MD 20742

Dr. J. D. Huba
Code 4780
Naval Res. Lab.
Washington, DC 20375

Dr. J. Lyon
Code 4780
Naval Res. Lab.
Washington, DC 20375

Dr. J. Giuliani
Code 4780
Naval Res. Lab.
Washington, DC 20375

Dr. S. Brecht
Berkeley Research Associates
P.O. Box 241
Berkeley, CA 94701

Dr. V. Thomas
Berkeley Research Associates
P.O. Box 241
Berkeley, CA 94701

Dr. H. Carl Fitz
Physical Research, Inc.
134 Holiday Ct., Suite 309
Annapolis, MD 21401

Dr. R. Armstrong
Mission Research Corp.
One Tara Blvd. Suite 302
Nashua, NH 03062

Defense Technical Information Center [2]
Cameron Station
Alexandrai, VA 22314

Dr. R. Henderson, W385
Director, JASON Program Office
The MITRE Corp.
7525 Colshire Dr.
McLeam, VA 22102

DASIAC
815 State St.
P.O. Drawer QQ
Santa Barbara, CA 93102

Dr. J. Kindel
MRC
127 Eastgate #20800
Los Alamos, NM 87544

Dr. T. Mazurek
Mission Research Corp.
P. O. Box 719
Santa Barbara, CA 93102

Dr. C. Longmire
Mission Research Corp.
P. O. Box 719
Santa Barbara, CA 93102

Dr. E. Witt
Mission Research Corp.
P. O. Box 719
Santa Barbara, CA 93102

Dr. J. R. Thompson
Austin Research Associates
1901 Rutland Dr.
Austin, TX 78758

Dr. J. M. Cornwall
Dept. of Physics
UCLA
Los Angeles, CA 90024

Dr. D. Hammer
Laboratory for Plasma Studies
809 Upson Hall
Cornell University
Ithaca, NY 14852

Dr. C. Prettie
Berkeley Research Associates
P.O. Box 241
Berkeley, CA 94701

Dr. J. Workman
Berkeley Research Associates
P.O. Box 241
Berkeley, CA 94701

Dr. D. Simons
ESS-7
MS D466

Dr. D. Sappenfield
ESS-7
MS D466

Dr. G. Smith
ESS-DOT
MS D446

Dr. M. Pongratz
ESS-DOT
MS D446